Available online at www.sciencedirect.com

ScienceDirect

Geochimica et Cosmochimica Acta 265 (2019) 292–312

Geochimica et Cosmochimica Acta

www.elsevier.com/locate/gca

Colloidal transport mechanisms and sequestration of U, Ni, and As in meromictic mine pit lakes

Konstantin von Gunten [a,*], Brendan Bishop [a], Isabel Plata Enriquez [a], Md. Samrat Alam [a,c], Peter Blanchard [b], Leslie J. Robbins [a,d], Renfei Feng [b], Kurt O. Konhauser [a], Daniel S. Alessi [a]

[a] Department of Earth and Atmospheric Sciences, University of Alberta, 1-26 Earth Sciences Building, Edmonton T6G 2E3, Canada
[b] Canadian Light Source, 44 Innovation Boulevard, Saskatoon, SK S7N 2V3, Canada
[c] Department of Earth Sciences, University of Toronto, 22 Russell St, Toronto, ON M5S 3B1, Canada
[d] Department of Geology and Geophysics, Yale University, 210 Whitney Avenue, New Haven, CT 06511, USA

Received 14 November 2018; accepted in revised form 5 September 2019; Available online 17 September 2019

Abstract

This study investigated the biogeochemistry of uranium (U), and the co-occurring elements nickel (Ni) and arsenic (As), in colloids and sediments from two meromictic mine pit lakes that have considerably different depths and geochemistry. In order to characterize the processes controlling metal speciation and cycling in the pits, the distribution and speciation of the elements in colloidal size fractions were analyzed using micro- and ultrafiltration in combination with transmission electron microscopy. Sediment traps collected fresh sediments over the course of one year below the chemocline of the pit lakes and were subsequently analyzed by scanning electron microscopy (SEM) for morphology and chemical digestions. The most common particles found in the shallower pit consisted of Ca-O and Fe-O colloids, while the particles in the deeper pit were composed of Ca-S-O. Filtration results showed a higher abundance of metals in larger colloidal fractions in aged samples, suggesting that colloids can act as metal accumulators. Sediment traps showed the formation of Fe-O, Fe-S, Al-Si, and Ce-P phases, which were observed to sorb U and Ni. The overall U removal was calculated to be 0.9 g/m^2/year in both pits, despite considerably different geochemical conditions between the two, and the maximum removal rates for As (shallow pit) and Ni (deeper pit) were 4.7 g/m^2/year and 0.6 g/m^2/year, respectively. Bottom sediments were also collected from both pits, and characterized using sequential extractions, SEM, synchrotron-based X-ray absorption spectroscopy and Laue diffraction techniques. These techniques showed that the stability of metals in the sediment follows the order Ni < U < As. Nickel, found in the exchangeable and acid soluble fractions, could be easily mobilized by changes in aqueous ionic strength and pH. Similarly, pH and redox changes in the water may strongly affect U, due to its dominance in the acid soluble and reducible sediment fractions. U(VI) mineral phases confirmed by spectroscopy and Laue diffraction, such as vandendriesscheite and monazite, which were likely associated with the oxidizable sediment fraction, may increase overall U stability. Arsenic was more strongly bound to the sediments and mostly present in the oxidizable and residual (highly recalcitrant) fractions. The collective results demonstrate the importance of colloidal particles for metal sequestration processes and their potential importance on microbial communities in pit lakes, highlighting the need for improved characterization of colloids in environmental studies.

Keywords: Uranium mining; Mine remediation; Colloidal pumping; Contaminant mobility; Metal speciation; Nanoparticles

* Corresponding author.
E-mail address: vongunte@ualberta.ca (K. von Gunten).

https://doi.org/10.1016/j.gca.2019.09.015
0016-7037/

1. INTRODUCTION

More than 180 meromictic pit lakes exist around the world in variable climates and geographical settings (Gulati et al., 2017). Such lakes have a permanently stratified deep water layer (monimolimnion) that does not mix with the upper water layer (mixolimnion). The development of this stratification is aided by the small surface area to maximum depth ratio, groundwater and surface water inflows and climatic factors (Pieters and Lawrence, 2014). Pit lakes, created by open pit mining, can become meromictic naturally or by artificially-induced means. In both cases meromixis can promote the removal of metal contaminants from the mixolimnion through metal and metalloid cycling at the chemocline, the highly dynamic boundary between the mixolimnion and the monimolimnion, which can have large physicochemical gradients. Metals can be transported from the mixolimnion into the monimolimnion and become trapped in the latter due to its permanent stratification, and eventually these metals can be sequestered into the pit bottom sediments due to saturation- or nucleation-induced precipitation (Soni et al., 2014; von Gunten et al., 2018). The development of anaerobic conditions within the monimolimnion can also promote the reductive immobilization of certain metal species. Overall, such mine pit lakes can sequester significant amounts of metals and metalloids in their sediments (Gulati et al., 2017). These can eventually become sources of contaminants themselves, thus impacting the quality of surrounding groundwater (Neves and Matias, 2008).

Colloid chemistry and interactions are critical aspects of metal and metalloid cycling, and understanding the extent to which colloids can sorb and transport metals is essential for determining their role in the functioning of meromictic pit lakes as a decommissioning measure. Colloids are generally defined as particles with a size range between 1 nm – 10 μm. Gustafsson and Gschwend (1997) further defined colloids as "any constituent that provides a molecular milieu into and onto which chemicals can escape from the bulk aqueous solution, while its vertical movement is not significantly affected by gravitational settling." This definition considers metals adsorbed and absorbed by non-settling mineral particles, humic substances, and non-motile microorganisms, but excludes metals complexed by organic acids, as those are generally considered to be truly dissolved. Colloidal particles can act as reaction centers, which lower kinetic energy barriers, as demonstrated by the reduction of U(VI) by small hematite colloids (Liger et al., 1999). Some metals, when sorbed to colloids, can be mobilized under conditions previously thought to prevent their mobilization, as shown for reduced and generally insoluble U(IV) in an anoxic environment of a uranium (U) contaminated peat bog (Wang et al., 2013). Similarly, Pu (III) and Pu(IV) mobility in natural aquatic systems was increased through colloidal transport and, consequently, less Pu was adsorbed to the solid phase (Nelson et al., 1985). The eventual accumulation of colloidal particles and subsequent formation of precipitating particulates can remove metals from the aqueous medium via a scavenging process referred to as "colloidal pumping" (Honeyman and Santschi, 1991; Dai et al., 1995). Such processes operate on longer time scales and can contribute to removal of metals from the mixolimnia of meromictic lakes, leading to an accumulation of trace metals in bottom sediments (von Gunten et al., 1997, Castro and Moore, 2000, Pelletier et al., 2009). This can, in turn, increase metal toxicity to benthic fauna (Cain et al., 2013; Croteau et al., 2013).

Although colloidal particles and their importance for metal and metalloid cycling has been investigated in rivers (e.g., Dai et al., 1995; Ross and Sherrell, 1999) and wetlands (e.g., Pokrovsky et al., 2005; Wang et al., 2013), studies regarding their behavior in lakes are limited (e.g., Gimpel et al., 2003). Colloidal metal transport is particularly understudied in artificial lacustrine systems, such as mining pits, where contaminant-loaded colloids may form more readily due to elevated concentrations of metals in pit water. These colloids may have high mobility in groundwater due to fractured, freshly weathered bedrock and a recently perturbed local hydrogeology (Ryan and Elimelech, 1996). In addition, colloidal abundance can increase due to local surface runoff and related soil disturbances. In a mining environment, revegetation during land reclamation may provide a fresh input of low molecular weight organic acids that can promote colloid formation (Slowey et al., 2007). Such organic acids can additionally liberate metals from waste rock, leading to a concomitant increase in metal concentrations and colloids.

To investigate colloidal processes and metal sequestration in meromictic lakes and their relevance as a decommissioning strategy, we studied two artificial meromictic pit lakes formed by open pit mining and located at the decommissioned Cluff Lake uranium mine in Northern Saskatchewan, Canada (Fig. 1). Today, these lakes, the shallower D-pit and the deeper DJX-pit, are distinct from each other in terms of both chemistry and geometry due to the host rock and ore geology, basin shape and mining and remediation history (von Gunten et al., 2018). A study by Dessouki et al. (2005) investigated the DJX-pit in its early stage of flooding and demonstrated that active fertilization and microbial growth could decrease contaminant metal concentrations in the mixolimnion. A more recent study investigated the aqueous biogeochemistry of the two pits and showed that some contaminants in the water were associated with Fe oxyhydroxides and Al-containing colloids (von Gunten et al., 2018). However, the nature of those colloids, their morphologies and their role in metal and metalloid sequestration has not been investigated. Furthermore, the contaminant sequestration potential and long-term stability in the sediments of the two pits is unknown. To further understand these relationships and their net effect on sequestration in reclaimed pit mines, we investigated the biogeochemistry of metal contaminants (with U, nickel (Ni), and arsenic (As) being of major concern) in the two pit lakes at Cluff Lake, using water filtrations, sediment traps, electron microscopy techniques, sequential extractions of bottom sediments (Tessier et al., 1979; Pichler et al., 2001; Kipp et al., 2009), and synchrotron-based X-ray spectroscopy and Laue diffraction. This study reveals how metal transport by colloidal particles can promote

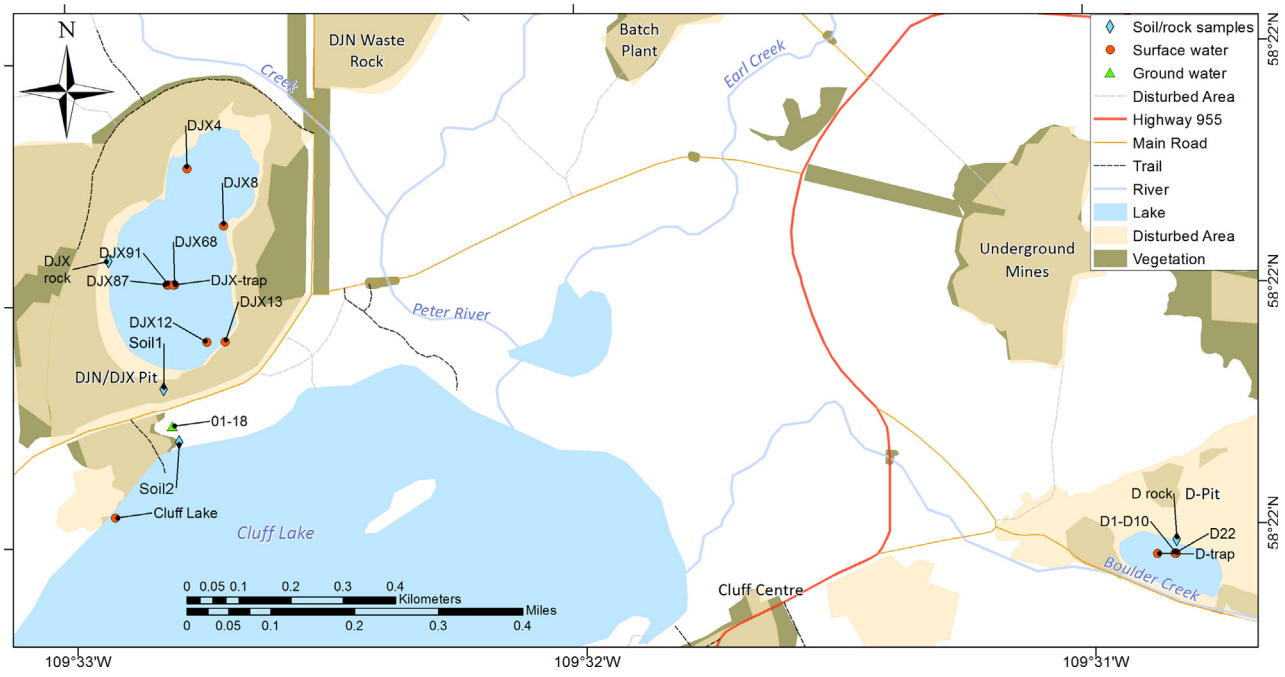

Fig. 1. Sampling locations in and around the two pit lakes (D-pit and DJX-pit) at Cluff Lake, northern Saskatchewan, Canada.

metal sequestration in pit lakes and provides estimates for metal removal rates in these systems. Furthermore, new insights into the stability of metals in sediments and important secondary minerals are discussed.

2. MATERIALS AND METHODS

2.1. Description of the pits

D-pit, the smaller of the two pits, has a maximum depth of 28 m and a surface area of 15 400 m^2. It was actively mined for U between 1979 to 1981, and eventually flooded in 1983 (AREVA, 2013). A chemocline is present at a depth of 13 m, with an anoxic monimolimnion below that has elevated pH values (pH 7.3–7.9) compared to the mixolimnion (pH 6.2–6.4). The major metals of concern in this lake were previously identified as U, with highest concentrations at the chemocline (up to 131 µg/L), and As, with up to 95 µg/L in the monimolimnion (von Gunten et al., 2018). The chemocline and the monimolimnion are influenced by Fe redox processes, suggesting that the biogeochemistry of the pit bottom is controlled by Fe(III) reduction.

The DJX-pit is deeper (91 m) and has a larger surface area (85900 m^2). It was mined periodically from 1989 to 1997 and allowed to flood in 2002 (AREVA, 2013). The lake in the DJX-pit lake has two major chemoclines, one at 18–20 m, and the second between 65 and 75 m, with stratification being controlled by carbonate dissolution and precipitation processes. Oxygen is present even near the bottom of the pit (0.9–1.9 mg/L; von Gunten et al., 2018), while the pH in the mixolimnion is neutral in contrast to the values in the monimolimnion (pH 5.6–6). The monimolimnion is dominated by sulfate (up to 476 mg/L), which is in contrast to the D-pit (<0.1 mg/L). Major metals of concern are U and Ni, with the highest concentrations in the deeper monimolimnion (1744 µg/L and 2193 µg/L, respectively). Other metals with elevated concentrations include Mn, Co, and Zn with concentrations up to 4 mg/L, 424 µg/L, and 687 µg/L, respectively. A regional groundwater model (AREVA, 2013) suggests some groundwater exchange between the DJX-pit and nearby Cluff Lake. Groundwater wells (e.g., Well 01–18 in Fig. 1) were installed between the two water bodies to monitor the groundwater quality. The trace metals U, As, and Ni are of primary concern in the two pits and were therefore the primary focus of this study.

2.2. Sampling

In June 2017, water samples were collected from the center of the D-pit and the DJX-pit from a boat using a MasterFlex E/S portable sampler (Cole-Parmer) and plastic tubing. Water was sampled from depths that were chosen to capture major geochemical changes along the chemoclines (von Gunten et al., 2018). Three depths were sampled in the D-pit: 5 m (mixolimnion), 13 m (chemocline), and 20 m (monimolimnion). Four depths were sampled in the DJX-pit: 5 m (mixolimnion), 20 m (upper chemocline), 40 m (upper monimolimnion), and 65 m (lower monimolimnion).

To investigate how metals, which may be transported by groundwater from DJX-pit towards a natural lake (Cluff Lake), are immobilized in a till-dominated soil, we collected soil samples and groundwater in the flow path between the two. The 9 m deep groundwater well 01–18, situated between DJX-pit and Cluff Lake (Fig. 1) was sampled with the MasterFlex E/S portable sampler after purging three

times the well volume according to Vail (2013). Saturated soil samples from the locations Soil1 (south of DJX-pit, depth 25 cm) and Soil2 (north of Cluff Lake, depth 80 cm) were collected in June 2018 using a hand shovel and transported in polypropylene centrifuge tubes. To understand the potential relationship between the geochemistry of U ores and resulting water chemistry, rock samples (D rock, DJX rock) were collected along the shores of both pits and U ore samples from Cluff Lake were analyzed as described below. Further details on the rock and ore samples are provided in the Supplementary Information (SI).

Bottom sediments were collected from the pit bottoms using an Ekman dredge. Samples from D-pit were retrieved in September 2015 from the middle of the pit and are hereafter referred to as D-1 to D-10 (Fig. 1). A new sediment sample was collected from 22 m depth in June 2017 and labeled D-22. Sediment samples from the DJX-pit were collected in June 2016 (shallow) and June 2017 (deep) from depths and locations provided in Table 1. The sediments were subsampled for analysis (n = 3), stored in polypropylene centrifuge tubes and placed on ice for transport back to the University of Alberta, where they were subsequently stored at –20 °C until further processing.

In June 2017, sediment traps were placed in D-pit and DJX-pit at 17 m and 47 m, respectively. These depths were selected to be below the upper chemoclines as identified by von Gunten et al. (2018). The sediment traps were constructed from 50 mL centrifuge tubes attached to a PET funnel (Fig. S10). An aluminum tube was attached below as a stabilizing weight. The rope holding the trap was attached to a buoy, which was attached to the center buoy in each pit. Plastic water logs held both buoys at a constant distance to prevent the ropes from becoming entangled. Both sediment traps were recovered after 374 days. In the DJX-pit, only approximately 25 mL of sediments were recovered and after detaching the funnel under water, the tube was capped and sealed with Teflon tape (Fig. S10). More than 50 mL sediments were found in the D-pit sediment trap, therefore, to prevent losses, the excess sediments with additional liquid was poured in additional 50 mL tubes, which were sealed as described above. Captured sediments were transported on ice. In the laboratory, samples were stored in an anaerobic glove box (98% N_2 and 2% H_2) prior to processing.

2.3. Colloidal size distribution and microscopy

To investigate the distribution of metals in different colloidal size fractions, aliquots of lake water were filtered on the boat immediately following sampling. Unfiltered aliquots were also collected for analysis. Dead-end filters (0.45 μm and 0.2 μm) were used for separating the larger size fractions, while reusable ultrafiltration cartridges (Pellicon XL, Millipore, 500 kDa and 10 kDa), both fed with the 0.2 μm permeate, were used for separating the smaller size fractions (Wang et al., 2013). The cartridges were flushed between the filtrations (50 mL 0.1 M hydrochloric acid, 50 mL 0.1 M sodium hydroxide, 50 mL of ultrapure water) and then preconditioned with at least 10 mL of the sample. Filtrations were performed differently in June 2017 and June 2018. The June 2017 filtrations were performed using syringes and syringe filters (Agilent) for larger size fractions. As there was a concern that the brief exposure to oxygen might alter the colloidal distribution, the filtrations were repeated in June 2018 using in-line filters (Waterra) prepared in a closed, sequential setup, in which permeate from one filter was subsequently fed into the next without air exposure. Using the same setup, groundwater from the well 01–18 (Fig. 1) was filtered in June 2018.

Previous studies on colloids have determined that changes in temperature can cause colloidal aggregation and agglomeration, ultimately leading to precipitation (von Gunten and Schneider, 1991; Tranvik, 1994). In pit lakes, such as those investigated here, colloids may be exposed to strong temperature changes at the chemocline and thermocline, for example, where the 4 °C water of the monimolimnion comes in contact with warmer surface water. To determine if this process affects the colloidal size distribution of metals in the two pit lakes, unfiltered water samples were collected in June 2017 at several depths into serum bottles using a nitrogen purged glove bag (Fisher Scientific) in the field (Wang et al., 2013). In order to age the

Table 1
Sediment and soil sample information: dates, depths and locations. Anoxic: anaerobically dried for XAS.

Sample name(s)	Location	Sampling date	Depth (m)	Anoxic
D-1 to D-10	D-pit	Sept 2015	not recorded	No
D-22	D-pit	June 2017	22	Yes
D-trap	D-pit	2017–2018	17	No
DJX-13a, DJX-13b	DJX-pit	June 2016	13	No
DJX-12a, DJX-12b	DJX-pit	June 2016	12	No
DJX-8	DJX-pit	June 2016	8	No
DJX-4a, DJX-4b, DJX-4c	DJX-pit	June 2016	4	No
DJX-68	DJX-pit	June 2017	68	No
DJX-87	DJX-pit	June 2017	87	No
DJX-91	DJX-pit	June 2017	91	Yes
DJX-trap	DJX-pit	2017–2018	47	No
Soil1	S of DJX-pit	June 2018	0.25	No
Soil2	N of Cluff Lake	June 2018	0.80	No

colloids, these samples were sealed and stored in an anaerobic glove box (98% N_2 and 2% H_2) at room temperature for one month. Samples were then filtered in the glove box following the same method as used in the field in 2017 (with syringes). After storing the water samples for 7.5 months in the glove box, precipitates were observed in samples from D-pit (20 m) and DJX-pit (65 m). The precipitates were retrieved by centrifugation (15000 *g*, 10 min) and dried at 60 °C. They were then carbon coated and analyzed by scanning electron microscopy coupled with energy dispersive X-ray spectroscopy (SEM-EDS) as described below.

All filtrates were diluted as necessary, acidified to a final concentration of 2% nitric acid, with the metals then being analyzed using an Agilent 8800 Triple Quadrupole ICP-MS as described in von Gunten et al. (2018). Size fraction ranges were calculated by using the differences between the larger and the smaller fractions. The June 2018 permeates were also analyzed for the total organic carbon (TOC; Shimadzu TOC-V analyzer) using the non-purgeable organic carbon method. To characterize colloidal particles, transmission electron microscopy (TEM; JEOL JEM-ARM200CF S/TEM) and energy dispersive X-ray spectroscopy (EDS) were performed using water from fresh samples collected in June 2017. Additional details on colloidal size distribution analysis are given in the SI.

2.4. Aqueous U speciation analysis

Because U and other redox sensitive metals have varying affinities toward colloidal particles depending on their speciation, it is important to investigate their oxidation states; however, this poses methodological challenges. Although thermodynamic speciation modeling is widely applied (e.g., Ramos et al., 2012), it cannot explain kinetically limited systems and is prone to large deviations from observations, especially when colloidal particles are involved (Gustafsson and Gschwend, 1997). In the two lakes studied here, the speciation of Fe and As was previously investigated using laboratory techniques (von Gunten et al., 2018), yet no data were obtained for U. To separate reduced from oxidized U in the field, we applied the method developed by Anderson (1984), which exploits the redox properties of U(III) and U(IV) that cause them to favorably co-precipitate with lanthanide fluorides, such as LaF_3 and NdF_3 under acidic conditions, leaving U(V) and U(VI) in solution (Foti and Freiling, 1964). Since other ions in the solution can compete with the fluoride anions, proper calibration of the assay is necessary. Additional details of these analyses are provided in the SI.

2.5. Bulk analysis of solid samples

Sediments from the sediment traps were mixed in their containers and the total volume was recorded. The dry masses of the solids were then determined by air-drying (under 98% N_2 and 2% H_2) for a week and weighing. Bottom sediment samples and soil samples were dried at 105 °C, sieved (<2 mm), and crushed using a mortar and pestle. Total carbon (TC), total organic carbon (TOC), and total nitrogen (TN) were analyzed by a Costech Model EA 4010 Elemental Analyzer. Total inorganic carbon (TIC) was calculated by subtracting TOC from TC. Microbial communities in the bottom sediments were investigated in both pits using 16S rRNA gene sequencing. These are described and discussed in detail in the SI.

Sequential extractions were performed on select bottom sediments and soil samples according to Tessier et al. (1979) and Li et al. (1995) to determine the elemental composition and distribution of various sediment fractions. All chemical digestion and extraction methods are described in detail in the SI. Briefly, the sequential extraction method differentiated between the following five fractions: (1) exchangeable, (2) carbonate-bound (acid soluble), (3) amorphous Fe-Mn-oxide-bound (reducible), (4) organic matter and sulfide-bound (oxidizable), and (5) residual. The final fraction was calculated by subtracting the concentrations of fractions 1–4 from the total concentration obtained by total digestion. Total digestion was performed by a wet digestion with nitric acid (HNO_3), hydrogen peroxide (H_2O_2), and hydrofluoric acid (HF). To prevent evaporation losses with HF for Si and As (Wang et al., 1997; von Gunten et al., 2017), a sodium hydroxide alkaline fusion with sodium peroxide was applied. During the extractions of a D-pit sediment (D-10), one sample was sacrificed after each extraction step for analysis by SEM-EDS (see below) to observe major changes in U. To distinguish between highly and poorly crystalline Fe compounds in the residual fraction, weak organic acid extractions with 7–35 mM oxalic and citric acids were performed (Borggaard, 1992; Joseph et al., 1996; Larios et al., 2013). Dried sediments from the sediment traps were finely ground and digested using the methods described above. All extraction and chemical digestion solutions were filtered through 0.2 μm nylon syringe filters and analyzed on an Agilent 8800 Triple Quadrupole ICP-MS.

2.6. Mineralogy, microscopy and spectroscopic analyses on solid samples

Bottom sediment subsamples for physical analyses were dried at 60 °C, sieved (<2 mm), and crushed using a mortar and pestle. Sediments from traps were dried at 25 °C. Mineralogy of the samples was analyzed on a Rikagu Ultima IV X-ray diffraction (XRD) unit with a cobalt X-ray source ($\lambda = 1.790260$). Data was interpreted using the JADE 9.5 software package and the databases: 2013 ICDD, 2015-1 ICSD.

In order to investigate the morphology of the sediments and potential U accumulation, selected sediments with high U concentrations from D-pit, DJX-pit, and both sediment traps were analyzed by SEM-EDS. For this purpose, bottom sediments were embedded into EPO-TEC 301 resin thin sections of 30 μm thickness on glass slides. Regions of U accumulation in the thin sections were identified using SEM-EDS (Zeiss EVO MA 15 and Sigma 300 VP-FESEM) as described in detail in the SI. Synchrotron-based X-ray analyses were performed at the Very Sensitive Elemental and Structural Probe Employing Radiation from a Synchrotron (VESPERS) beamline at the Canadian Light

Source (CLS) in Saskatoon, Canada with thin sections from selected D-pit and DJX-pit sediments, and powder samples for bulk analysis (Feng et al., 2007, 2010). Micro-X-ray fluorescence (XRF) maps of the thin sections were collected using a polychromatic X-ray beam with an energy range of 2–30 keV and a beam spot size of ~3 μm. Samples were mounted in the focus of the X-ray beam at an angle of 45° from the horizontal plane. XRF spectra were collected with a single element silicon drift detector (Vortex-90EX; HITACHI) positioned 45° to the incident X-ray beam in horizontal plane. Laue diffraction patterns were collected from selected U hotspots using a Dectris Pilatus 1 M Pixel Array Detector positioned 90° to the incident X-ray beam in vertical plane. Visualization of the maps and correlation calculations between elements (Pearson's linear product-moment correlation) were done using MATLAB R2015b. The Laue diffraction patterns were analyzed using the XMAS v.6 software (Tamura, 2014).

Micro X-Ray Absorption Near Edge Structure (μ-XANES) at the U L_{III}-edge, As K-edge, and Ni K-edge were measured in fluorescence mode using a four-element silicon drift detector (Vortex-ME4, HITACHI). The energy of incident X-ray were scanned using a double crystal Si(111) monochromator ($\Delta E/E = 10^{-4}$). The detector was positioned 90° to the incident X-ray beam in horizontal plane. Samples were positioned in the focus of the incoming X-ray beam at an angle of 45° in both the vertical and horizontal directions. Five to six μ-XANES scans were collected for each hotspot. Bulk XANES spectra were collected using a bigger beam of 0.8 mm × 0.8 mm in size. For bulk XANES, Teflon holders with a 3 mm slot in the middle were used. Ground sediment samples were packed into the slot and secured with Kapton tape on both sides. Samples were again positioned in front of the incident X-ray beam at a 45° angle with the fluorescence detector positioned 90° relative to the incident X-ray beam in horizontal plane. Bulk XANES measurements were performed at the U L_{III}-edge and the As-K edge using either a four-element Vortex silicon drift detector or a liquid nitrogen cooled 13-element germanium detector (Canberra). For each sample, 5–10 scans at a spot with the highest absorbance at the corresponding edge energy were performed. Post-processing of the XANES spectra was performed using Athena (Demeter 0.9.24 XAS Processing Software; Ravel and Newville, 2005). The spectra were corrected by the energy shift, normalized, and compared to standard XANES spectra using linear combination fitting (see SI for more details on VESPERS-related analyses). As there was a concern that the drying procedures might influence sediment mineralogy, selected sediment samples from June 2017 were dried at room temperature in an anaerobic chamber containing 98% nitrogen and 2% hydrogen. The dried sediments were then immediately processed for XRF and μ-XANES as described above.

To verify the findings obtained by VESPERS, electron microprobe analyses were performed using a CAMECA SX100 microprobe. Selected carbon coated slides from each pit (bottom sediments) with known U grain locations (from SEM-EDS) were used. Additional EDS and wavelength dispersive X-ray spectroscopy were performed to differentiate the overlapping X-ray peaks of S, Pb, As, and Mg.

3. RESULTS

3.1. Water samples

3.1.1. Colloidal distribution of elements

In D-pit, total U concentrations increased from the surface to the chemocline at 13 m to 130–160 μg/L and decreased again to about 50% of the chemocline value at 20 m depth (Fig. 2). The majority of U in fresh samples was in the dissolved form. Arsenic gradually increased with depth to 40–90 μg/L and was distributed over all size fractions. Closer to the surface, larger As-bearing colloids dominated the size fractions, especially those in the 500 kDa-0.2 μm range. Overall, lower concentrations of As were detected in June 2018 and a dominance of the 500 kDa-0.2 μm fraction was observed. This difference could be attributed to oxidation processes during the brief sample exposure to the atmosphere that might have occurred in June 2017. Iron in the D-pit was distributed in a similarly diverse way as As, ranging up to 51–53 mg/L in total, which suggests a similar mechanism of colloidal immobilization. Low concentrations of Ni were detected in the D-pit (<10 μg/L), with most of it being associated with the <10 kDa size fraction, with some contributions of the larger 10 kDa-0.2 μm fractions.

U in the DJX-pit also increased with depth and reached a peak of 1–1.7 mg/L at a depth of 65 m and was dominantly associated with the <10 kDa fraction. Nickel similarly gradually increased up to 1.3–1.9 mg/L, with the majority of it being in the <10 kDa fraction, indicating the dominance of small colloids and dissolved species. In June 2018, colloids in the range of 10–500 kDa carrying Ni were found. Concentrations of As and Fe were low in the DJX-pit (1 μg/L and <161 μg/L, respectively), making it impossible to resolve the colloidal distribution.

A markedly different size distribution was observed for the aged samples that were filtered after one month of storage at room temperature under anaerobic conditions (Fig. 2). In the case of U in the D-pit surface water sample, the smaller 500 kDa − 0.2 μm size fraction became more dominant than the 0.2–0.45 μm size fraction, which was opposite of the result observed for the fresh samples. The distribution of As in the larger fractions (0.2–0.45 μm and >0.45 μm) modestly increased for all tested D-pit depths. Ni in the D-pit became abundant in the 10–500 kDa fraction. Iron became more abundant in the <10 kDa colloidal fraction, replacing the larger 10–500 kDa and 500 kDa-0.2 μm fractions that were important in the fresh samples. For aged DJX-pit samples, in some cases more than 50% of U was detected in the larger colloidal fractions, especially the 500 kDa-0.2 μm size fraction, again in contrast to the fresh samples. Colloidal Ni > 10 kDa only started to emerge at a 6–10% contribution, as compared to between 0–2% in fresh 2018 samples that was primarily due to 0.2–0.45 μm and >0.45 μm fractions. Besides the major elements of concern, Mo and Al showed notable changes in colloidal distribution. Molybdenum (up to 86 μg/L) showed a similar distribution to U, especially in the matured samples (up to 40% colloidal), which indicated that Mo and U are exhibiting similar chemical behavior in the

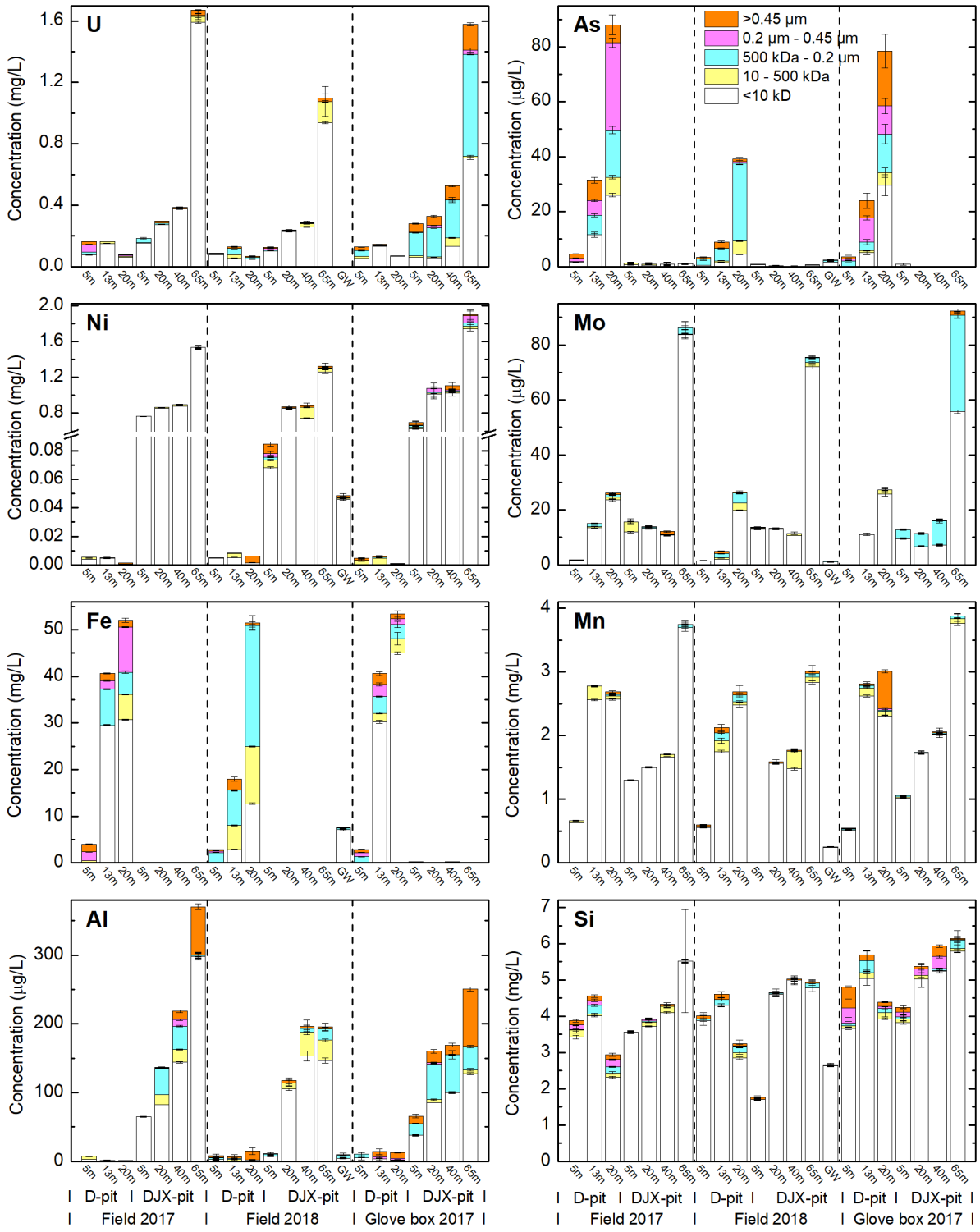

Fig. 2. Colloidal size fractionation results for selected metals. The data is grouped by sampling date and pit (D-pit, DJX-pit). The error bars represent instrumental errors (ICP-MS, n = 3). Note y-axis breaks for Ni (elevated in the DJX-pit). Data on other elements can be found in Tables S26–S28.

DJX-pit. Aluminum in the mature samples was present in the larger colloidal fractions and in much lower concentrations as compared to fresh water, indicating the aggregation of smaller Al-bearing colloids and the precipitation of Al-containing phases.

Filtration results from the groundwater well 01–18 indicated that the major water chemistry is similar to the surface water of the DJX-pit (Fig. 2, Table S28), specifically for concentrations of Mg, S, K, and Ca. This supports the hydrogeological model (see AREVA, 2013) that sug-

gested groundwater flow from the DJX-pit towards Cluff Lake. Trace metals, such as Ni, Mo, and Mn, were only present in the <10 kDa fraction, implying that the aquifer between DJX-pit and Cluff Lake was efficiently removing colloid-bound metals. Similar aquifer filtering properties were found by Hollings et al. (1999) in groundwater at the Rabbit Lake uranium mine. No U was detected in the water sample from groundwater well 01–18.

3.1.2. Observed precipitates

D-pit precipitates collected from the 20 m sample after the 7.5 month aging experiment (Fig. 3 and Table S23) were rich in Fe and O, with an average Fe/O molar ratio of 0.2. This ratio most closely matched the iron hydroxide mass ratio of a hydrous ferric oxide such as ferrihydrite ($Fe(OH)_3$; Fe/O: 0.3). The lower ratio could be explained by residual water in the sample and the presence of other oxides. DJX-pit precipitates were more diverse. The particles shown in Fig. 3 were rich in Al and Si (8.1 wt% and 10.0 wt%, respectively) and contained minor amounts of Mg (1.1 wt%), K (2.4 wt %), and Fe (1.2 wt%). Based on the Al/Si, Al/K, and Si/K molar ratios, the precipitates are similar to kaolinite ($Al_2Si_2O_5(OH)_4$) and muscovite ($KAl_3Si_3O_{10}(OH)_2$), which were both also found in the deep (>68 m) sediments of the DJX-pit. Some particles showed a high abundance of S (10.1 wt %) and Ca (12.2 wt%) and may be attributed to the precipitation of gypsum ($CaSO_4{\cdot}2H_2O$).

3.1.3. Shape and bulk chemistry of colloids

S/TEM confirmed the presence of colloidal particles in D-pit at depths of 5 m, 13 m, and 20 m, and in DJX-pit at 60 m and 65 m, with colloidal particles ranging in size from 20-300 nm. EDS mapping on selected colloids (Fig. 4) revealed major differences between colloidal particles present in the two pits. Colloidal particles found in the D-pit were dominated by Fe-O and Fe-O-Ca phases, with minor occurrences of Si-O in the 13 m water sample, while in the DJX-pit, colloids were mostly Ca-O and Ca-O-S phases. Although the DJX-pit water is depleted in Fe, Fe-O particles were detected. Arsenic, Ni, and U concentrations were below the detection limit for S/TEM-EDS imaging of the colloidal particles. No carbon-dominated colloids were detected, suggesting a minor role of organic matter colloids in the two pit lake systems. Filtrations and TOC analysis of June 2018 samples confirmed the lack of larger carbon particles in the D-pit and DJX-pit surface samples, but showed some 10–500 kDa C particles in deeper layers of both pits (Fig. S7), suggesting that some C-rich colloids might be present at these depths having a similar size distribution as As and Fe.

3.1.4. Aqueous U speciation

In the surface water of the D-pit, both extraction techniques (with Ca and without) demonstrated that U(VI) was the dominant species (Table S22). The results obtained with the Ca calibration curve suggest higher U(VI) abundance and seem more reasonable, as the top water layers of D-pit were well mixed and oxidized and only small amounts of U(IV) would be expected. At the chemocline, where the redox conditions change, a transition from U (VI) to U(IV) was observed and the monimolimnion was dominated by U(IV). The results for DJX-pit, which does not become anoxic below the chemocline unlike the D-pit, suggest that no U(IV) was present in the mixolimnion and the upper monimolimnion (i.e., DJX-pit water samples from 5 m, 20 m, and 40 m depths). In the 65 m sample, about 72% of U was in the U(IV) form.

For some samples, less U precipitated than would be expected for a pure U-Ca solution based on the calibration curves. This resulted in some U(VI) values in excess of 100% (127–176%). The presence of certain dissolved species may interfere with the precipitation behavior of U in the sample solutions. For example, it is likely that Mg, Sr, and traces of lanthanides (e.g., Ce) being released from the solid phase (Table S15) are also competing for F^-, and unlike Ca, they were not included in the calibration. In addition, the presence of organic matter and stable colloids might further influence the calibration and results. Uranium is known to co-precipitate with Ca (Perry et al., 1981), which makes it difficult to isolate the effect of Ca during NdF_3 co-precipitation. Moreover, replicating the sample solution chemistry in the simulated solutions used to make up calibration standards is especially challenging. For these reasons, the obtained results should be inter-

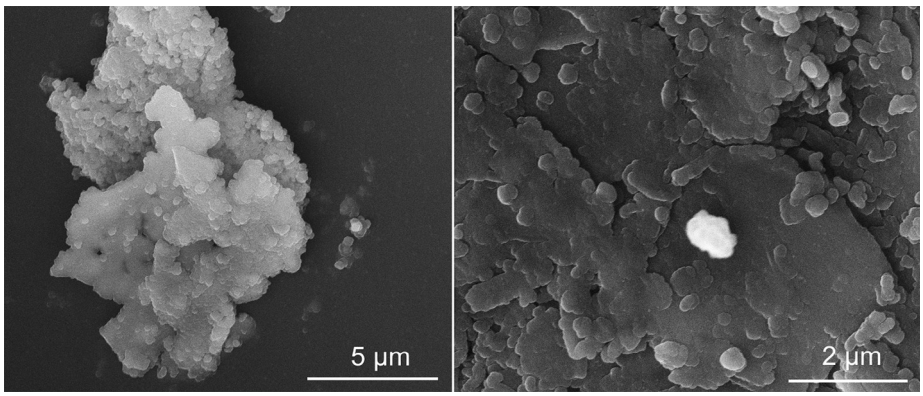

Fig. 3. Selected SEM images of precipitates formed at room temperature after 7.5 months from D-pit (left) and DJX-pit (right) from 20 m and 65 m water depth, respectively. For EDS composition see Table S23. For D-pit sample consider spot numbers 18–22. For DJX-pit sample consider spot number 52.

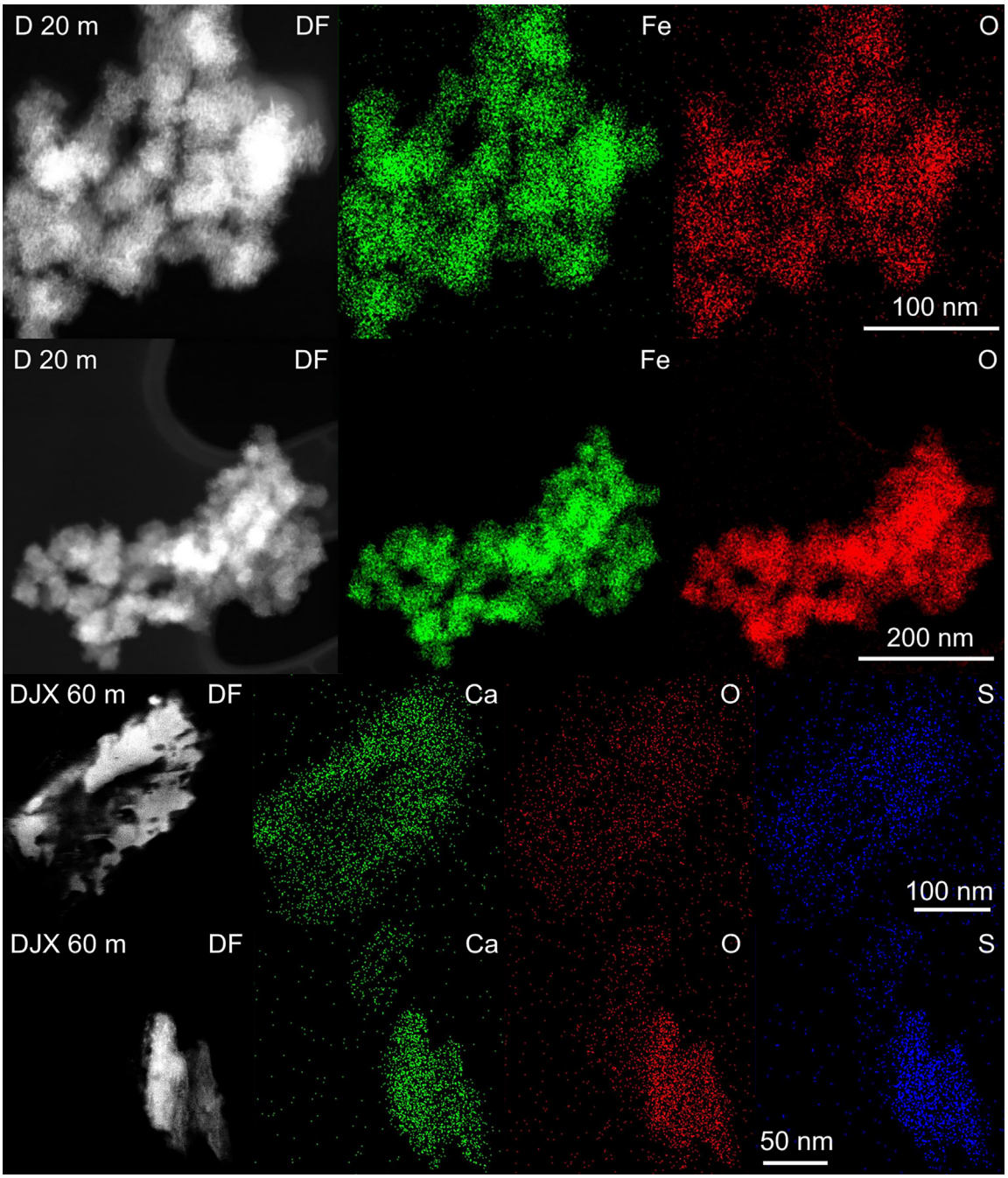

Fig. 4. Selected TEM images of colloids found in fresh water in D-pit (top) and DJX-pit (bottom).

preted with caution, and viewed qualitatively rather than as a strict quantitative measure of the abundances of U(IV) and U(VI).

3.2. Bottom sediments

3.2.1. Sediment mineralogy and chemistry

In the bottom sediments, abundant feldspar minerals were identified, including anorthite, albite, orthoclase, and microcline (Table S2). The latter three were predominantly found in DJX-pit samples. Clay minerals present included muscovite, clinochlore, kaolinite, and illite, with the latter primarily found in DJX-pit, whereas hematite and dolomite were present mostly in D-pit samples. Only a few samples had TC abundances >1% (i.e., D-6: 1.5%, DJX-13a: 2.0%, DJX-8: 4.2%, DJX-4a: 1.2%, and DJX-68: 1.0%). In these samples, the TC was dominantly present as TOC.

The distribution of elements in the sediment fractions as determined by sequential extraction showed substantial differences between the two pits, and within DJX-pit large variations between sample pools (deep vs. shallow) were also observed (Fig. 5, details in Tables S3–S12). The major

elements of concern in both pits, U, As, and Ni, were found in concentrations ranging from 40–1630 μg/g, 10–450 μg/g, and 100–240 μg/g, respectively. These elevated sediment concentrations can be explained by the oxidation and weathering of surrounding bedrock and waste rock (Tables S2 and S15) containing minerals, such as uraninite and traces of niccolite, and bravoite (von Gunten et al., 2018). In both pits, U was mainly present in three fractions: a carbonate (acid soluble) fraction (28–77% of total U), an amorphous Fe/Mn oxide (reducible) fraction (17–50%), and a residual fraction (1–41%). The Fe/Mn oxide (reducible) fraction was identified as the major U-bearing phase in deep sediment sample DJX-68 (32–50%), while in shallow samples, U was mainly in the carbonate fraction

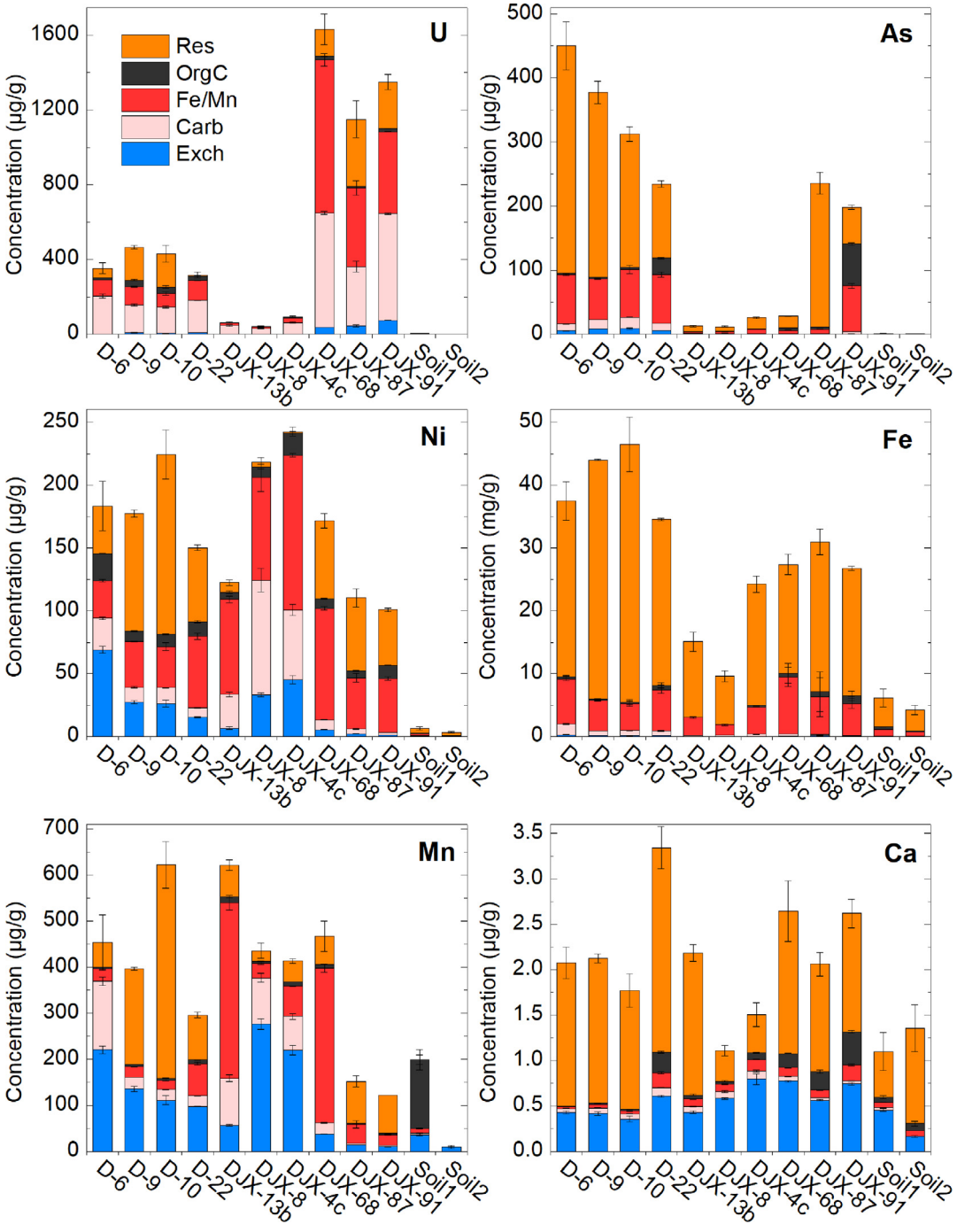

Fig. 5. Sediment sequential extraction summary for U, As, Ni, Fe, Mn, and Ca. Fraction, from least to most recalcitrant are: exchangeable (Exch), acid soluble carbonates (Carb), reducible Fe/Mn oxide (Fe/Mn), oxidizable organic matter/sulfide (OrgC), and the residual fraction (Res). The error bars represent 1 standard deviation (n = 3). Data on more elements can be found in Tables S3–S12.

(67–77%). The residual fraction was less substantial in the shallow DJX-pit samples (4–13 m depth) with only 1–2% of total U bound in this phase.

Although not abundant in the water of DJX-pit, As was present at similar total concentrations in D-pit and the deep DJX-pit sediment samples. Arsenic was identified mainly in the residual fraction (29–95%) of the sediments from both pits, followed by the amorphous Fe/Mn oxide fraction (3–36%). However, DJX-91 had a relatively large organic matter/sulfide fraction for As (33%). Phosphorus had a noticeably similar distribution, as well as total concentrations, to that of As (Tables S3–S12), suggesting comparable chemical behavior.

Nickel, although present in only trace levels in D-pit water, had similar total concentrations in the sediments as compared to the DJX-pit samples. Similar to other transition metals (Cu, Co, Mn) and S, a considerable fraction of the total concentration was found in each of the five sediment fractions. In the D-pit and shallow DJX-pit samples, Ni had a notable presence in the highly mobile, exchangeable fraction (5–38%) and the acid soluble carbonate fraction (5–42%). The more resilient reducible Fe/Mn oxide fraction contained 15–62% Ni. Ni in the residual fraction was only substantial in D-pit and deep DJX-pit samples, with concentrations varying between 36–64%.

Iron and Ca are important indicators for Fe/Mn oxides and carbonates, which is why their speciation should also be considered. Iron was consistently present in the residual fraction (74–88%) with a smaller contribution from the amorphous Fe/Mn oxide (reducible) fraction (9–33%). Calcium was mainly present in the residual fractions (28–76%), except for shallow sediments from the DJX-pit, where the exchangeable fraction contained more Ca (20–53%).

Extractions with citric and oxalic acids performed on sediments D-6 and D-9, showed that with 18–35 mM acid, U and As could be extracted in greater abundances than by sequential extraction steps 1–4 (Table S16). This indicates that some of the U and As assigned to the residual fraction in the sequential extractions may be associated with poorly crystalline Fe oxide compounds. This was observed for up to 100% of U and up to 35% of As in the residual fraction, but not for Ni.

3.2.2. Bulk XANES

Linear combination fitting of synchrotron U L_3-edge XANES data of bulk sediment samples showed that the majority of U in the D-pit in the sediments was U(VI) (85%), with the remaining 15% being U(IV) (Tables S18-S19). Similar results were found in the DJX-pit for the samples DJX-13a, DJX-8, and DJX-4c, with an average value of 79% for U(VI) and 21% for U(IV). Arsenic K-edge XANES for D-pit samples indicated that a little more than half (58%) was present as reduced As(III), while the remainder was As(V) (Table S20). The As(III) proportion in the DJX-pit sediments was, on average, 29%.

3.2.3. SEM-EDS, μ-XANES and Laue diffraction on U-hotspots

SEM-EDS analysis on sediments collected from the pits detected U-rich grains ranging in size from 5-50 μm, exam-

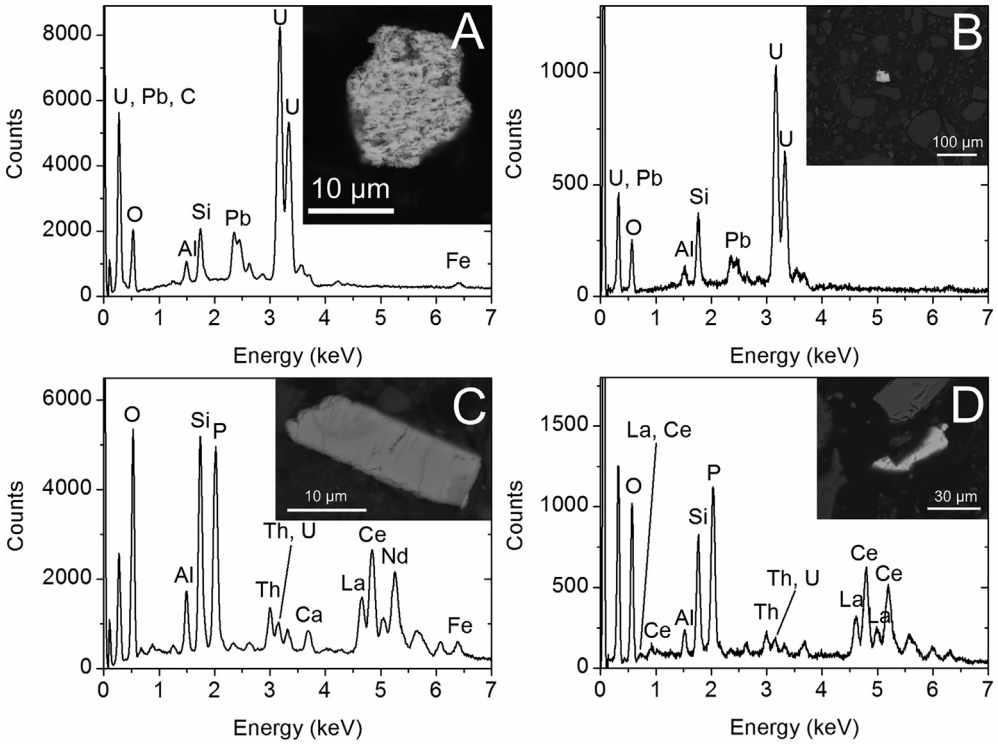

Fig. 6. Examples of U-rich grains detected by SEM-EDS. Top: U-Pb accumulations found in samples D-10 (A) and DJX-4c (B). Bottom: monazite grains found in samples D-6 (C) and DJX-13a (D).

ples of which are shown in Fig. 6. A summary of the grain composition (Table S17) is provided in the SI. EDS analysis indicated that U-rich grains predominantly consisted of O (37–72%), U (3–22%), and Pb (1–3%). In three grains, up to 3% Ti was detected. Four grains contained traces of U and were identified as monazite-(Ce), represented by the chemical formula (Ce, La, Nd, Th)PO_4. In such grains, Th(IV) can be partially substituted with U(IV) (van Emden et al., 1997). Sequential extraction of the sediments indicated that the U-rich grains were dissolved in the fourth extraction step (hydrogen peroxide and ammonium acetate), as shown in Fig. S4, suggesting that the U was associated with the oxidizable sediment fraction.

Contrary to bulk XANES results (Fig. S1), U L_3-edge μ-XANES (Fig. 7; Fig. S1) on the identified U-grains from D-pit samples indicated that, on average, 67% of the U was present as U(IV) with the remaining 33% as U(VI) (Table S18). Results from anaerobically dried sediments were similar to those obtained for air dried samples. For the shallow DJX-pit sediments, 44% U(IV) was measured (Table S19). Arsenic K-edge μ-XANES indicated that the U hotspots in D-pit samples mounted on glass slides yielded a generally higher proportion of As(III) (on average 78%) as compared to the quartz slides (on average 45%), as shown in Table S20, likely due to background As in the glass slides having an As(III) fraction of 70%. This means that only quartz slide samples provided reliable μ-XANES data for As. For one DJX-pit U hotspot (quartz glass) the data were of sufficient quality to perform fitting, and the As(III) fraction averaged 33%. Therefore, similar to the bulk samples, the hotspots generally displayed a relatively strong reduced component that corresponded best with As(III), with the remaining As component fit to As (V). Although Ni is not known to be redox sensitive under common environmental conditions, and the concentration of Ni was fairly low in the U accumulations, Ni XANES fitting was attempted for four U-hotspots in sample D-10 (Table S21). The averaged XANES curves indicate various Ni(II) binding environments in the sediments, however, we were not able to resolve them further (Fig. S3).

In D-pit grains, U correlated strongly with Pb (79%), Th (63%), and As (69%) (Tables S18–S19). The correlation of U with Ni was, on average, 54%, and correlations with Ca and Fe were generally low (22% and 16%, respectively). In the DJX-pit grains, the correlation between elements was lower. Uranium correlations with Pb, Th, and As were 41%,

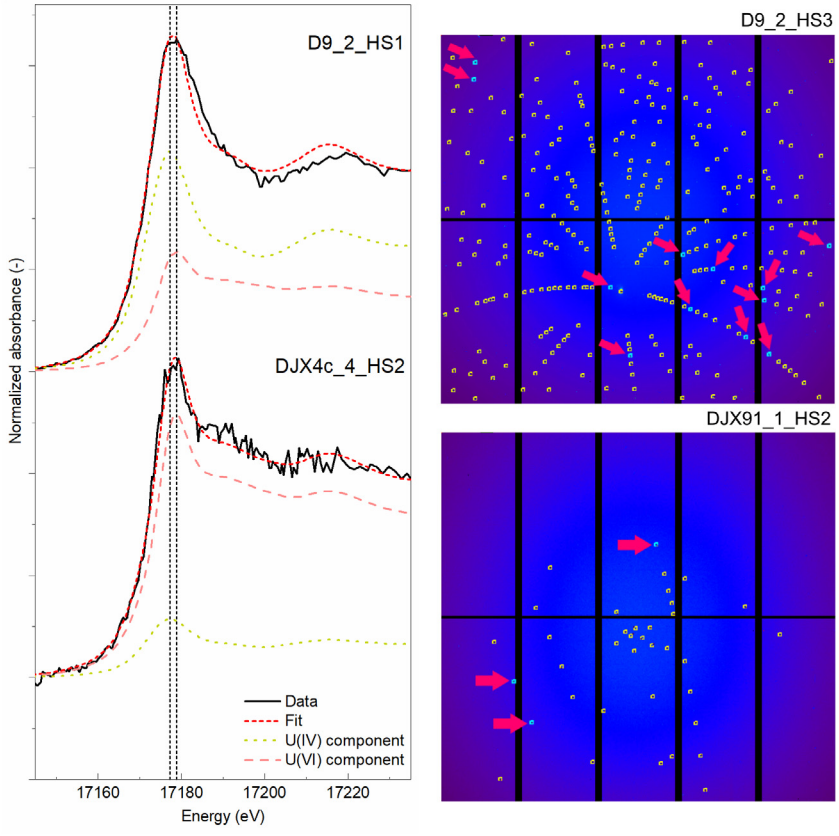

Fig. 7. VESPERS fit data and Laue diffraction patterns. Left: examples of U L_3-edge XANES fits on the U hotspots D9_2_HS1(D-pit bottom sediments, unknown depth) and DJX4c_4_HS2 (DJX-pit bottom sediments, 4 m depth). The averaged data (solid line, black), obtained fit (dashed, red) and the fit components (dotted and dashed, green and pink) are shown. See Fig. S1 for more examples. Right: indexed Laue diffraction patterns for D9_2_HS3 and DJX91_1_HS2 using the vandendriesscheite crystal structure. Not fitted reflections are colored bright blue and marked with arrows. (For interpretation of the references to colour in this figure legend, the reader is referred to the web version of this article.)

14%, and 45%, respectively. Correlations between U and Fe or Ni in the DJX-pit were similar to grains from the D-pit; however, the correlation between U and Ca was higher for DJX-pit grains (46%).

Indexations of Laue diffraction patterns from U minerals (Fig. 7) yielded satisfying results for the mineral vanden-driesscheite, a lead uranyl oxic hydrate ($Pb(UO_2)_{10}O_6(OH)_{11}\cdot 11(H_2O)$), with a similar crystal structure to metaschoepite (Burns, 1997). For several grains, a better indexation was obtained for gauthierite, another lead uranyl oxic hydrate ($KPb[(UO_2)_7O_5(OH)_7]\cdot 8H_2O$) (Olds et al., 2017). Results were similar for sediments from both pits (Tables S18 and S19). Microprobe analysis with wavelength dispersive X-ray spectroscopy confirmed that the U-rich grains were generally abundant in Pb, but not S or As (Figs. S5 and S6). The occurrence of Ti in some grains was additionally confirmed.

3.3. Soil samples

Sequential extractions on soil samples collected between DJX-pit and Cluff Lake showed generally low metal abundances compared to the sediment samples. For example, the soil closer to DJX-pit (Soil1) only contained 6.4 μg/g U and 6.6 μg/g Ni. In this sample, the majority of U (52%) was found in the carbonate-bound fraction, followed by the Fe/Mn oxide fraction (30%), similar to the sediments (Table S13). Nickel and Co were mostly bound to the residual fraction (58% and 59%, respectively), followed by the Fe/Mn oxide fraction (22% and 23%, respectively). They were therefore not as mobile as in the pit sediments where the exchangeable fraction was larger. Closer to Cluff Lake (Soil2), even lower concentrations of U and Ni were recorded at 0.5 μg/g, and 3.4 μg/g, respectively (Table S14). In this sample, U was found dominantly in the residual fraction (47%), followed by the carbonate-bound fraction (25%) and the Fe/Mn oxide fraction (21%). Nickel (and Co) were distributed similarly to sample Soil1.

3.4. Sediments from sediment traps

3.4.1. Sediment quantification and chemistry

The sediment traps yielded a total 2.3 g and 0.6 g of dry sediments from D-pit and DJX-pit, respectively, after 374 days of deployment. Thus, using a sediment trap area of 95 cm^2 (Fig. S10), average deposition rates of 6.6 g/m^2/day (D-pit, 17 m) and 1.7 g/m^2/day (DJX-pit, 47 m) were calculated. In general, the water chemistry matched a system in equilibrium with the fresh sediments in the two pits (Table 2). D-pit sediments were found to be rich in As, Fe, and Mn, compared to the DJX-pit sediments, which in turn, were more concentrated in bulk elements such as Al, Ca, K, Mg, S, and the trace elements Co, Cu, Mo, Ni, Zn, and U.

3.4.2. Mineralogy and SEM-EDS

SEM-EDS analyses on the sediments from sediment traps revealed that D-pit sediments were dominated by Fe oxide and Fe sulfide phases (Fig. 8). In addition, monazite-like grains were detected, which contained lanthanides (e.g., La, Ce, Nd) and the actinide Th. These grains are similar to those that were previously described in the bottom sediments of the two pits. In DJX-pit, Fe was not as dominant as in D-pit. Instead, many clay-like particles were detected. Additionally, Fe sulfide particles (Fig. 8) were detected, some of which contained Ni (up to 3.9%) and Co (up to 5.0%). One particle, having a composition similar to an aluminosilicate, showed detectable amounts of U (0.3%), suggesting that those silicates are capable of sorbing U from the pit water. Monazite-like grains, enriched in light-weight lanthanides were also observed in the DJX-pit.

Table 2
Concentrations of selected elements in the sediment traps (per g dry weight) and the corresponding total mass deposited within one year based on a calculated deposition rate shown in the bottom line. For more elemental concentrations, see Table S15.

	D-pit		DJX-pit	
	μg/g	g/m^2/year	μg/g	g/m^2/year
Al	15,100	36.1	47,300	29.8
As	1950	4.67	55.3	0.0349
Ca	5440	13.0	7460	4.70
Co	17.0	0.0405	460	0.290
Cu	17.6	0.0420	255	0.160
Fe	223,000	534	45,100	28.4
K	5310	12.7	20,400	12.8
Mg	2880	6.88	15,300	9.61
Mn	2250	5.39	1890	1.19
Mo	19.1	0.0456	207	0.131
Ni	46.5	0.111	896	0.565
P	793	1.90	640	0.403
Pb	15.8	0.0377	29.3	0.0185
S	3830	9.16	20,900	13.2
U	378	0.903	1450	0.913
Zn	12.7	0.0303	176	0.111
Rate (g/m^2/year)		2390		630

4. DISCUSSION

4.1. Colloidal transport

The distribution of colloidal metals suggests that in the fresh water samples the majority of trace metals, such as U and Ni, were in the dissolved form or associated with small colloids (<10 kDa). Arsenic, on the other hand, was associated with colloids >10 kDa, likely Fe oxyhydroxides, as suggested by similar colloidal size distribution. These results are similar to those reported by Hollings et al. (1999), who investigated the colloidal fractions in waters at the Rabbit Lake U mine. They found that U, Ni, and As in water with little disturbance (e.g., deeper layers of tailings pond) were mostly in the fraction <0.02 μm, i.e., likely truly dissolved. In the current study, S/TEM-EDS results indicated that the colloidal pool in D-pit is dominated by Fe-O particles, whereas in DJX-pit, colloids are mostly composed of Al-Si-Ca-S-O particles. Colloidal aging at room temperature for one month led to a general shift towards larger colloids and a decrease in metal concentra-

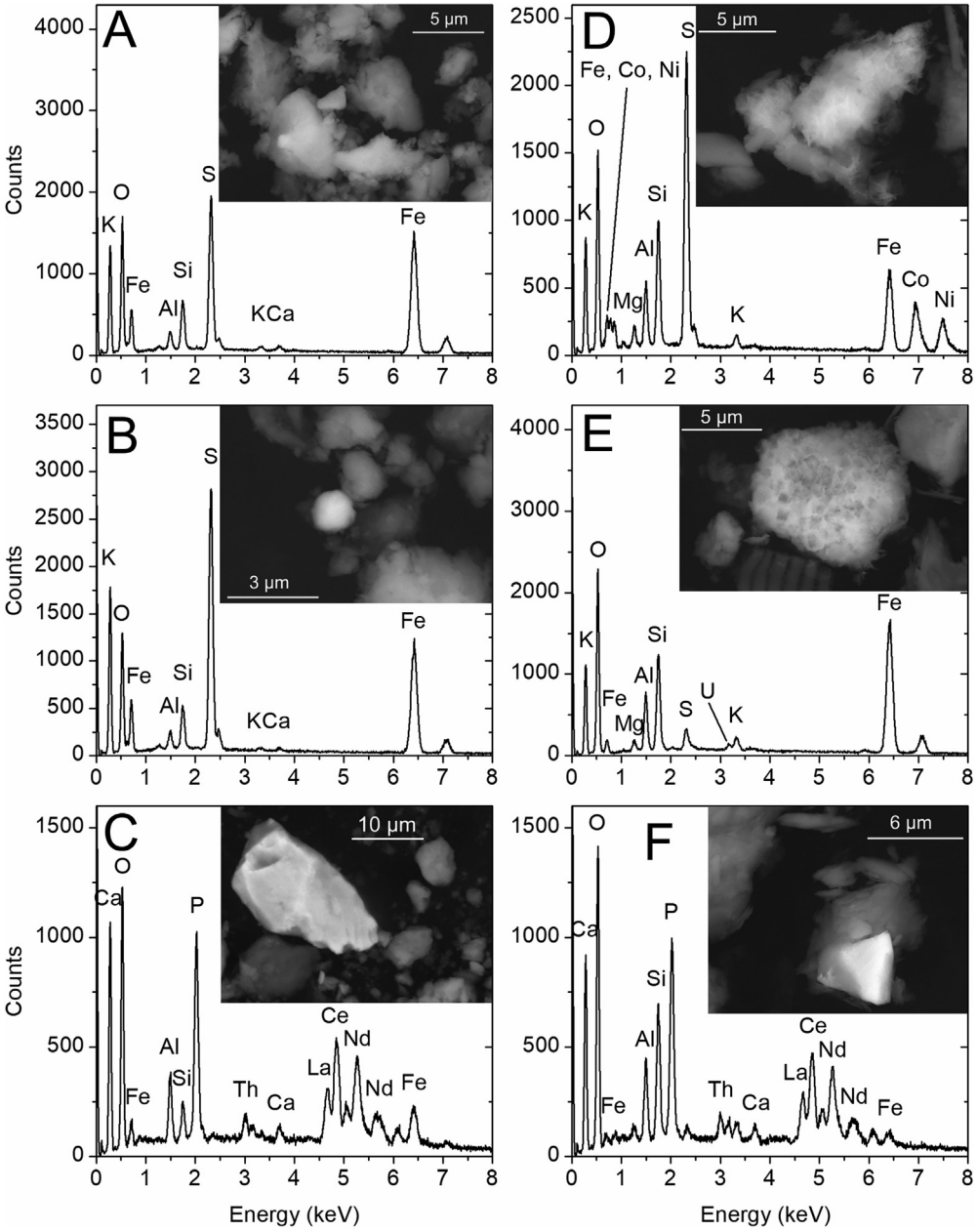

Fig. 8. SEM-EDS images on selected spots found in the sediments collected by sediment traps in the D-pit (A, B, C) and DJX-pit (D, E, F). C and F show potential grains of monazite-(Ce). D and E show grains containing Ni, Co, and U. EDS results on those and other grains are summarized in Table S24.

tions, presumably the result of flocculation and subsequent precipitation (Fig. 1). Such shifts are likely to happen in the pits with time, when colloidal particles are exposed to different temperature conditions, especially at the thermoclines (in close proximity to the chemoclines) where warmer surface water is in contact with deeper, colder water. As suggested by the colloidal pumping theory (Dai et al., 1995), larger aged colloids are more prone to being removed from the water column.

As observed in incubated water bottles and the sediment traps, sediments forming over time in D-pit were dominated by Fe oxyhydroxides (Fig. 9). In DJX-pit, the sediments were chemically similar to minerals such as kaolinite, muscovite, and gypsum, the latter being predicted to form in the water column based on thermodynamic modeling (von Gunten et al., 2018). Gypsum is known to form in leachates in contact with dolomitic host rocks (Gupta and Singh, 2003), which is the case for both pits. Despite the obvious chemical differences between the pits, our observations suggest that primarily Fe sulfide phases are efficient in removing trace metals, such as U, Co, and Ni, from the water column below the chemocline. This process is known and

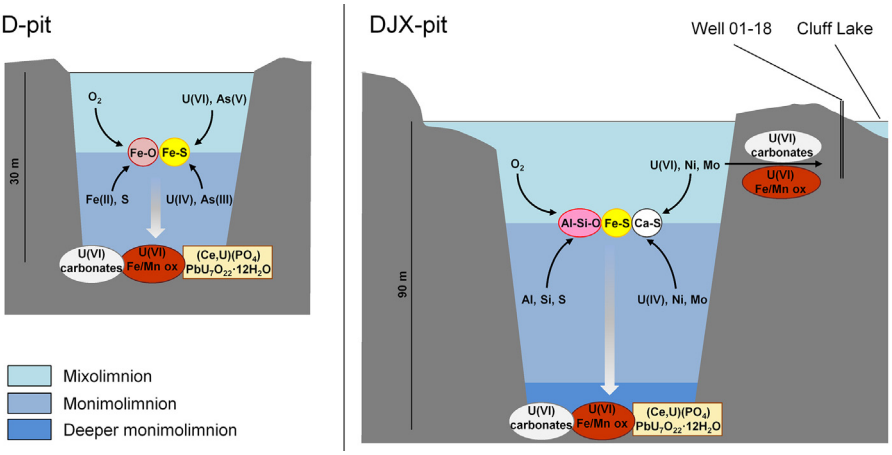

Fig. 9. Schematic diagram of colloid formation and transport processes and the corresponding phases and minerals in the two pit lakes D-pit and DJX-pit. Note: schematic is not to scale.

was previously described in mining affected lakes (Huerta-Diaz et al., 1998) and groundwater (Saunders et al., 2018). Based on calculations done using data from the sediment traps (Table 2), we can estimate that the removal of U from the water column in both pits is very similar, 0.9 g/m^2/year at the corresponding depths, even though the U concentrations above the deployment depths in the two pits are clearly different, e.g., <131 mg/L and <307 mg/L in D-pit and DJX-pit, respectively (von Gunten et al., 2018). As the DJX-pit sediment trap was deeper and the pit has higher aqueous U concentrations, one may expect a higher rate of U accumulation. However, it is likely that other U removal processes (discussed below) in addition to the above-discussed removal by Fe-S phases, occur in the D-pit, contributing to an overall higher removal efficiency. Fe-S phases could also play an important role in the sequestration of other contaminants, such as As and transition metals, through sorption and co-precipitation (Yang et al., 2016; Saunders et al., 2018). Sequential extractions did not show significant amounts of oxidizable As, Ni (Fig. 5) or other transition metals, e.g., Co and Cu (Table S12) in the bottom sediments, fractions that would correspond to amorphous sulfides (Tessier et al., 1979). However, most of those metals are largely present in the residual fraction, suggesting that crystalline sulfides might be a potential sink (Poulton and Canfield, 2005).

In D-pit, Fe-O phases may play an important role in trace metal and metalloid cycling. Such Fe-O might sorb As (up to 4.7 g/m^2/year, Table 2) and with it U, as U is known to bind to arsenate phases (Gupta and Singh, 2003). Tang and Reeder (2009) observed an increased affinity of U(VI) to aluminum oxides pretreated with As(V). Such coated Al particles are likely to form in the D-pit environment, where an Al removal rate was calculated as 36.1 g/m^2/year. In addition, at the investigated sediment trap depths, more U(IV) might be expected in D-pit compared to DJX-pit, as suggested by the oxidation state measurements of U. Here, U may be present as U(IV) hydroxide, as the environmental conditions (i.e., ORP: −263 mV, pH: 7.9; von Gunten et al., 2018), would favor this species (Langmuir, 1978). In addition, the high abundance of Fe(II) in D-pit supports the presence of U(IV), as Fe^{2+} has been shown to reduce U (Du et al., 2011), favoring its accumulation and precipitation.

In DJX-pit, the removal of U by aluminosilicates (Wilmarth et al., 2006), which was previously hypothesized by von Gunten et al. (2018), could indeed be taking place. Aluminosilicates were observed in the collected sediments (Fig. 8), and Al and U were found in similar colloidal size distributions, especially in the deep and aged DJX-pit water samples (Fig. 2). In addition to U, Mo is also precipitating in DJX-pit (0.1 g/m^2/year) and it is known that Mo oxyanions behave in a chemically similar manner to U oxyanions (Brassier-Lecarme et al., 1997). Previous studies have indicated that U and Mo both strongly sorb to organic matter and clay minerals (Morrison and Spangler, 1992), supporting the hypothesis that aluminosilicates could be removing U in DJX-pit. Additionally, under the presence of Fe and Mn within oxic/suboxic conditions, the formation of Fe/Mn oxyhydroxides can contribute to the removal of scavenged Mo (Algeo and Tribovillard, 2009). Indeed, some Fe-O colloids were observed in the DJX-pit by S/TEM-EDS, suggesting that this process might be taking place in the deep, oxygen-limited DJX-pit water layers. Although phosphate fertilization experiments by Dessouki et al. (2005) did not show an increase in Mo precipitation, due to the low affinity of Mo to biogenic particles (e.g., algae), our observations suggest that Mo might be affected by colloidal pumping because of the sorption to inorganic colloidal particles.

In the aged D-pit sample, Ni shifted from mostly dissolved species towards colloidal particles of 10–500 kDa, thereby increasing the potential for Ni removal which was calculated to be around 0.1 g/m^2/year. This process likely contributes to the low concentration in the monimolimnion of the D-pit. Although present in much higher concentrations in DJX-pit, the removal of Ni was only 6 times larger, 0.6 g/m^2/year. Nickel removal in DJX-pit is likely limited due to the prevalence of dissolved Ni, even in the stored and aged samples, which was likely contributed by the lower pH conditions in the monimolimnion. This observa-

tion is also supported by the low concentrations of Ni and its near absence in the residual fraction within the shallow sediments of the DJX-pit (Fig. 5).

4.2. Sequestration of metals in the sediments

Metals and metalloids precipitating out of the water column will eventually accumulate in pit lake bottom sediments (Laird et al., 2014), where their speciation will ultimately determine their environmental fate. The strong presence of U in the carbonate fraction suggests the presence of uranyl carbonates (Vandenhove et al., 2014) or the incorporation of U in carbonate minerals (Tessier et al., 1979, Abdelouas et al., 1998). However, the fundamentally different distribution of Ca compared to U, and XRD results, do not suggest a significant presence of Ca-bearing carbonates. No carbonate crystals with sorbed or co-precipitated U were found by either SEM-EDS or Laue diffraction. Similarly, Vandenhove et al. (2014) did not observe any correlation between $CaCO_3$ and U within the carbonate fraction. Instead, this U may be present in the form of uranyl carbonates or hydrated carbonates that are adsorbed to the surface of silicate minerals (Abdelouas et al., 1998). Uranium in this carbonate fraction can be considered stable under many environmental conditions due to the low solubility of carbonate minerals under neutral to basic pH conditions (Troyer et al., 2014). Such conditions prevail in the D-pit, where neutral pH values exist at the bottom (von Gunten et al., 2018). However, in DJX-pit, the pH is more acidic (pH 5.6 below 20 m), which may lead to the remobilization of solid and suspended carbonates in this lake. In the DJX-pit, however, the Fe/Mn oxide and residual fractions play a more significant role for U sequestration. Accordingly, the Fe/Mn oxide fraction may represent U sorbed to amorphous Fe/Mn oxide, while the residual fraction might represent U incorporated into more recalcitrant, crystalline Fe oxides, such as hematite (Tessier et al., 1979, Sheppard and Thibault, 1992; Duff et al., 2002). Hematite was detected in most D-pit and some DJX-pit samples (Table S2). The high abundance of U in the Fe/Mn oxide fraction in the deep DJX-pit samples compared to D-pit can be explained with the oxic/suboxic conditions in the deep monimolimnion, which differs from the anoxic monimolimnion of D-pit (von Gunten et al., 2018). Therefore, this Fe/Mn oxide fraction might release U upon the establishment of anoxia in DJX-pit.

Troyer et al. (2014) investigated U tailings and mining affected stream and pond sediments (North Cave Hills, South Dakota, USA) and found that most U was in the acid soluble carbonate fraction and the reducible Fe oxyhydroxide fraction, which is similar to findings of this study. However, at the toe of the tailings pile, Troyer et al. (2014) found that the exchangeable fraction was dominant. In our study, the exchangeable fraction was rather low, suggesting that the sediments do not contain easily mobilized U. In the two pit lakes at Cluff Lake, the acid soluble (carbonates) and Fe/Mn oxide oxides fractions contributed the most to the U pool in the sediments, which on average accounted together for 78% of total U (Tables S3–S12).

Arsenic, which was dominant in the two most resilient fractions (Fe/Mn oxides and residual), should be stable within the sediments. A similar distribution and total concentrations of As were reported by Troyer et al. (2014). Pichler et al. (2001) analyzed the distribution of metals in the tailings of another U mine in northern Saskatchewan and found that As was bound to amorphous Fe oxyhydroxides rather than to crystalline Fe oxides or residual fractions. In the Cluff Lake pits, the amorphous Fe oxide phase was generally not as important for As as compared to the residual fraction. Similarities in the distribution of As and P can be explained by their similar chemical behavior and the possibility of phosphate and arsenate co-precipitation (Dungkaew et al., 2012). The observed similarities with respect to Fe distributions, would further suggest that As and P are competing for sorption sites on Fe oxides (Hongshao and Stanforth, 2001).

Similar Ni, Co, and Mn distributions are likely the result of these metals being associated with Mn oxides (Larsen and Postma, 1997). Perhaps surprisingly, Ni was not especially abundant in the deeper sediment samples in DJX-pit, compared to the Ni-poor D-pit. Complexation with sulfate and the depressed pH conditions in the DJX-pit promoted Ni remaining in solution (Larsen and Postma, 1997), an interpretation consistent with previous thermodynamic modeling (von Gunten et al., 2018). The lower pH values of the deeper DJX-pit layers (>20 m) could also decrease the abundance of Ni within the exchangeable fraction in those sediments, as lower pH values may lead to a decrease in the abundance of negatively charged surface sites available for Ni^{2+} sorption. Notable is the absence of Ni in the residual fraction in shallow DJX-pit sediments.

Sediment chemistry is directly linked to microbial community compositions (see SI for details). Deeper sediment communities generally have lower species richness and species diversity, likely attributable to higher metal and metalloid concentrations and the decreasing abundance of electron acceptors such as O_2, NO_3^-, and SO_4^{2-}. Sediment TOC and Fe concentrations correlating with the bottom sediment communities in the D-pit, whereas in the DJX-pit, U concentrations were likely an important driver.

4.3. Importance of the U micro-grains

Both minerals identified in the U-rich grains, vandendriesscheite and gauthierite, are alteration products of a uraninite precursor, which has been found in U mines such as the Shinkolobwe mine in Congo (Burns, 1997; Olds et al., 2017) and the Jáchymov mine in Czech Rebuplic (Ondrus et al., 1997). The majority of the grains were classified as vandendriesscheite, an early alteration product (Plášil, 2014), which has the lowest concentration of Pb (originating from the radioactive decay of U) of all lead oxide hydrates (Burns, 1997). According to Burns (1997), due to the accumulation of Pb, this alteration product requires long-term exposure to oxidizing conditions, and therefore, it is unlikely that this mineral formed during the sample recovery and preparation. As some grains did not show any identifiable Laue diffraction pattern or pro-

duce a satisfactory fit to a known mineral standard (Table S18), it can be inferred that some form of non-crystalline uraninite was present (Alessi et al., 2014), an assertion confirmed by XANES spectra which indicated that the predominant oxidation state of U was 4+, with 44–67% U(IV). Bacterial U reduction in the sediments of the pits might be limited, as traces of oxygen (0.9 mg/L) and nitrate (1.6 mg/L) in the DJX-pit might be responsible for the suppression of potential U(VI) reducing organisms (Finneran et al., 2003). In D-pit, high abundances of Fe oxides might suppress microbial U(VI) reduction through competition of U(VI) and Fe(III) as electron acceptors (Wielinga et al., 2000). Therefore, it is likely that the observed micro-crystals of vandendriesscheite and gauthierite are the result of the alterations of detrital uraninite or amorphous pitchblende in the mining pits, which were exposed to wet and oxic conditions over 4 years, i.e., during the mining operations and initial flooding. The dominance of As(III) in those grains and the high correlation between As and U (Tables S18–S20) are consistent with previous findings as vandendriesscheite, and similar uraninite alteration products, can contain up to 1.7% As_2O_3 impurities (Deditius et al., 2007). It also suggests that the grains are not highly matured, as it has been observed that over time As(III) and As(-I) in flooded mine tailings are generally oxidized to As(V) and form stable arsenates, such as scorodite ($FeAsO_4{\cdot}2H_2O$) (Warner and Rowson, 2007). This phase was, however, not identified in our samples. The U-rich micro-grains seem to generally promote the overall stability of U, as suggested by the sequential extractions and corresponding SEM-EDS analyses.

Over time, in the Ca- and Si-rich environments of the D-pit and DJX-pit water-sediment-boundary (von Gunten et al., 2018), the vandendriesscheite (and possibly gauthierite) grains could be expected to form uranophane ($CaU_2Si_2O_{11}{\cdot}6H_2O$) and masuyite ($PbU_3O_{10}{\cdot}3H_2O$) assuming no kinetic barriers (Finch and Ewing, 1991). Masuyite can further alter to curite ($Pb_3U_8O_{27}{\cdot}6H_2O$), kasolite ($PbUSiO_6{\cdot}H2O$), and soddyite ($U_2SiO_8{\cdot}2H_2O$) in the presence of silica (Finch and Ewing, 1991). The uranyl silicate minerals are generally less soluble than uranyl oxic hydrates or uranyl carbonates (Gorman-Lewis et al., 2008), which would be beneficial for U stability in the pit sediments. Furthermore, curite would promote the precipitation of uranyl phosphates (Finch and Ewing, 1991), which are even more insoluble than uranyl silicates (Gorman-Lewis et al., 2008). Uranyl phosphates would be more favored in the slightly acidic environment of DJX-pit deeper water, although, the formation of the required curite may be suppressed (Plášil, 2014). In D-pit, on the other hand, although the formation of curite might be favored, the precipitation of phosphates and/or arsenates could be suppressed by the elevated pH conditions characteristic in the D-pit (Plášil, 2014).

4.4. Limitations and recommendations

Besides the previously discussed difficulties in determining U speciation, further limitations should be considered. First, sediment samples were collected using a grab sampler from a boat, which provides an averaged sample over a sediment depth of approximately 5–10 cm. Repeated sampling in the D-pit performed in September 2015 indicated potentially large variations in the total concentrations of major metals and metalloids, mostly contributed by differing size distributions of sampled particles. However, the relative distribution of the elements over the five solid fractions was always similar (see Figs. S12 and S13), suggesting that the metal/loid speciation was relatively homogeneous. Still, our sampling method only allowed for a bulk analysis (i.e., not a depth-resolved analysis) of geochemical gradients within the pit sediments. Second, while the standard deviation between subsamples (e.g., shown in Fig. 5) did not suggest substantial variation within each solid sample, our sampling techniques likely overlook important gradients in the microbial communities within the sediments (Rogozin et al., 2017) and the formation of geochemical microenvironments where specific mineral phases might form (e.g., Brantner et al., 2014). Third, sediment traps in the water columns of the pits were deployed over a period of more than a year, which allowed us to average out seasonal variations and changes in stratification patterns. However, the extended sampling period allowed for early diagenesis/mineralization processes to take place (Meyers and Ishiwatari, 1993). Those processes may alter the observed concentrations of TOC, TN, P, and metabolically involved trace metals because of their mobilization from the sediments by microbial processes (Bloesch and Burns, 1980). Although long sampling periods are not uncommon for low-productivity systems (e.g., Hobbs et al., 2010), future sediment trap studies should consider shorter sampling periods or at least a split between the open-water period (approximately May-September) and the ice-covered period (Minnow Environmental, 2019). Such seasonal investigations could be also combined with the analysis of colloidal fractions. In our study, water was only sampled in June, however, AREVA (2013) and von Gunten et al. (2018) have shown that the pits are highly variable and developing systems. Although concentrations of elements in the water column and the major stratification patterns were not shown to vary significantly between June and September, they may vary substantially during the ice-covered period, as temperature changes can alter colloidal distribution (von Gunten and Schneider, 1991). Fourth, it is critical to better understand the meromictic behavior of the two pits. For example, the presence of oxygen in the monimolinmion of the DJX-pit remains unexplained. Its depletion might cause dramatic future changes in metal/loid sequestration and speciation in sediments. Future studies could include the deployment of automatic data loggers at various depths to determine the source and seasonality of oxygen in this pit, and develop a better understanding of the surrounding hydrogeology, which would aid in making better predictions of the development of meromixis in these and other artificial or natural lakes.

5. CONCLUSIONS

The study by von Gunten et al. (2018) deomonstrated the importance of the Fe redox cycle for the distributions of U and As in the D-pit. Iron oxyhydroxide formation

and dissolution at the chemocline promote U(VI) reduction and U(IV) oxidation by Fe(II) and Fe(III) species, respectively, a process that causes a U concentration maximum near the chemocline. For the DJX-pit, the same study proposed that the Ca carbonate cycle might be involved in the stratification of the DJX-pit (around the upper chemocline). Furthermore, it was proposed that colloids could contribute to the removal of contaminants in both pit lakes. Our observations here confirm those previous findings and help to elucidate the interactions between colloidal-bound and dissolved contaminants. For example, our observations support metal sequestration by colloidal particles in the pits by the colloidal pumping process (Fig. 9). Trace metals accumulate onto colloidal particles, such as the newly-discovered Ca-O and Fe-O particles in the D-pit, and Ca-S-O particles in the DJX-pit. Colloidal aggregation and precipitation can then lead to the removal of metals from the water column, a process that was observed during the laboratory incubation of pit water samples. Additionally, we observed that in the two investigated pits, Fe-S particles were able to sorb trace metals, such as Ni and Co. Aluminosilicates were found to sorb U in the DJX-pit environment, as was previously suggested by von Gunten et al. (2018). Although different in their water chemistry, both pits express a similar precipitation rate for U below the chemocline of about 0.9 g/m^2/year. Our results also provide insights into the environmental stability of contaminants sequestered in the pit bottom sediments, which is summarized as Ni < U < As. Nickel, having large exchangeable and acid soluble fractions, could be easily mobilized by changes in the ionic strength and acidity of the water. Similarly, pH and redox changes in the water may strongly affect U in the acid soluble and reducible sediment fractions. Observed U mineral phases, such as vandendriesscheite, might promote U stability over longer periods of time. Continuous monitoring of the pit will allow observation regarding the environmental stability moving forward, and if necessary, identify if intervention is required to counter any environmentally detrimental development. This study demonstrates the importance of the colloid/sediment interactions in mine pit lakes and their potential influence on microbial communities and metal mobility, which has significant implications for the metal and metalloid cycling in other mining sites that involve open pit mining and that aim to use pit lakes and bioremediation techniques as decommissioning strategies. Results presented here indicate that colloidal fractions with particle sizes > 0.45 μm might be overlooked when applying standard monitoring techniques and might not reveal the full extent of metal distribution in pit lake environments.

Declaration of Competing Interest

The authors declare that they have no known competing financial interests or personal relationships that could have appeared to influence the work reported in this paper.

ACKNOWLEDGEMENTS

Orano Canada Inc (formerly AREVA Resources Canada) and Canada North Environmental Services Limited Partnership (CanNorth) facilitated site access and sampling procedures, and provided historical sampling data. University of Alberta Northern Research (Canada) financially supported field-related activities. CLS financially supported the work at the VESPERS beamline with travel awards to K. von Gunten and S. Alam. L. Robbins gratefully acknowledges the support of a Vanier Canada Graduate Scholarship. K. Konhauser and D. Alessi [grant numbers: EGP 511159-17, RGPIN-04134] were supported by Natural Sciences and Engineering Research Council of Canada Engage and Discovery Grants. We are grateful for initial microbiological investigations on the sediments by Christopher Boothman and Jonathan Lloyd. We also appreciate scientific advice from Gabrielle Dublet and the technical support during sample processing and analysis by Weiduo Hao, Neil MacPherson, Cheng Zhong, Guangcheng Chen, Nathan Gerein, and Andrew Locock. We thank the three anonymous reviewers for their valuable input that helped to improve our study.

APPENDIX A. SUPPLEMENTARY MATERIAL

Supplementary data to this article can be found online at https://doi.org/10.1016/j.gca.2019.09.015.

REFERENCES

Abdelouas A., Lutze W. and Nuttall E. (1998) Chemical reactions of uranium in ground water at a mill tailings site. *J. Contam. Hydrol.* **34**(4), 343–361.

Alessi D. S., Lezama-Pacheco J. S., Stubbs J. E., Janousch M., Bargar J. R., Persson P. and Bernier-Latmani R. (2014) The product of microbial uranium reduction includes multiple species with U (IV)–phosphate coordination. *Geochim. Cosmochim. Acta* **131**, 115–127.

Algeo T. J. and Tribovillard N. (2009) Environmental analysis of paleoceanographic systems based on molybdenum–uranium covariation. *Chem. Geol.* **268**(3), 211–225.

Anderson R. F. (1984) A method for determining the oxidation state of uranium in natural waters. *Nucl. Instr. Meth. Phys. Res.* **223**(2–3), 213–217.

AREVA (2013) Cluff lake project: 2012 annual report. AREVA Resources Canada Inc.

Bloesch J. and Burns N. M. (1980) A critical review of sedimentation trap technique. *Schweiz. Z. Hydrol.* **42**(1), 15–55.

Borggaard O. K. (1992) Dissolution of poorly crystalline iron oxides in soils by EDTA and oxalate. *J. Plant. Nutr. Soil Sci.* **155**(5), 431–436.

Brantner J. S., Haake Z. J., Burwick J. E., Menge C. M., Hotchkiss S. T. and Senko J. M. (2014) Depth-dependent geochemical and microbiological gradients in Fe (III) deposits resulting from coal mine-derived acid mine drainage. *Front Microbiol.* **5**, 215.

Brassier-Lecarme C., Baron P., Chevalier J. L. and Madic C. (1997) Acidic organophosphorus solvent extraction process for the purification of molybdenum in tailings from uranium ore treatment. *Hydrometallurgy* **47**(1), 57–67.

Burns P. C. (1997) A new uranyl oxide hydrate sheet in vandendriesscheite: Implications for mineral paragenesis and the corrosion of spent nuclear fuel. *Am. Mineral.* **82**(11–12), 1176–1186.

Cain D. J., Croteau M. N. and Fuller C. C. (2013) Dietary bioavailability of Cu adsorbed to colloidal hydrous ferric oxide. *Environ. Sci. Technol.* **47**(6), 2869–2876.

Castro J. M. and Moore J. N. (2000) Pit lakes: their characteristics and the potential for their remediation. *Environ. Geol.* **39**(11), 1254–1260.

Croteau M. N., Cain D. J. and Fuller C. C. (2013) Novel and nontraditional use of stable isotope tracers to study metal bioavailability from natural particles. *Environ. Sci. Technol.* **47** (7), 3424–3431.

Dai M., Martin J. M. and Cauwet G. (1995) The significant role of colloids in the transport and transformation of organic carbon and associated trace metals (Cd, Cu and Ni) in the Rhône delta (France). *Mar. Chem.* **51**(2), 159–175.

Deditius A. P., Utsunomiya S. and Ewing R. C. (2007) Alteration of UO 2+ x under oxidizing conditions, Marshall Pass, Colorado, USA. *J. Alloys Compd.* **444**, 584–589.

Dessouki T. C., Hudson J. J., Neal B. R. and Bogard M. J. (2005) The effects of phosphorus additions on the sedimentation of contaminants in a uranium mine pit-lake. *Water Res.* **39**(13), 3055–3061.

Du X., Boonchayaanant B., Wu W. M., Fendorf S., Bargar J. and Criddle C. S. (2011) Reduction of uranium (VI) by soluble iron (II) conforms with thermodynamic predictions. *Environ. Sci. Technol.* **45**(11), 4718–4725.

Duff M. C., Coughlin J. U. and Hunter D. B. (2002) Uranium co-precipitation with iron oxide minerals. *Geochim. Cosmochim. Acta* **66**(20), 3533–3547.

Dungkaew W., Haller K. J., Flood A. E. and Scamehorn J. F. (2012) Arsenic removal by precipitation with Calcium phosphate hydroxyapatite. *Adv. Mat. Res.* **506**, 413–416.

Feng R., Dolton W., Igarashi R., Wright G., Bradford M. and McIntyre S. (2010) Commissioning of the VESPERS beamline at the Canadian light source. *AIP Conf. Proc.* **1234**(1), 315–318.

Feng R., Gerson A., Ice G., Reininger R., Yates B. and McIntyre S. (2007) VESPERS: A beamline for combined XRF and XRD measurements. *AIP Conf. Proc.* **879**(1), 872–874.

Finch R. J. and Ewing R. C. (1991) Alteration of natural uranyl oxide hydrates in Si-rich groundwaters: Implications for uranium solubility. *Mater. Res. Soc. Symp. Proc.* **257**, 465–472.

Finneran K. T., Johnsen C. V. and Lovley D. R. (2003) Rhodoferax ferrireducens sp. nov., a psychrotolerant, facultatively anaerobic bacterium that oxidizes acetate with the reduction of Fe (III). *Int. J. Syst. Evol. Microbiol.* **53**(3), 669–673.

Foti S. C. and Freiling E. C. (1964) The determination of the oxidation states of tracer uranium, neptunium and plutonium in aqueous media. *Talanta* **11**(3), 385–392.

Gimpel J., Zhang H., Davison W. and Edwards A. C. (2003) In situ trace metal speciation in lake surface waters using DGT, dialysis, and filtration. *Environ. Sci. Technol.* **37**(1), 138–146.

Gorman-Lewis D., Burns P. C. and Fein J. B. (2008) Review of uranyl mineral solubility measurements. *J. Chem. Thermodyn.* **40**(3), 335–352.

Gulati, R. D., Zadereev, E. S. and Degermendzhi, A. G. (eds.) (2017) *Ecology of Meromictic Lakes*. Springer, Cham, Switzerland.

Gupta C. and Singh H. (2003) *Uranium Resource Processing – Secondary Resources*. Springer, Berlin, Heidelberg.

Gustafsson C. and Gschwend P. M. (1997) Aquatic colloids: concepts, definitions, and current challenges. *Limnol. Oceanogr.* **42**(3), 519–528.

Hobbs W. O., Lalonde S. V., Vinebrooke R. D., Konhauser K. O., Weidman R. P., Graham M. D. and Wolfe A. P. (2010) Algal-silica cycling and pigment diagenesis in recent alpine lake sediments: mechanisms and paleoecological implications. *J. Paleolimnol.* **44**(2), 613–628.

Hollings P., Hendry M. J. and Kerrich R. (1999) Sequential filtration of surface and ground waters from the Rabbit Lake uranium mine, northern Saskatchewan, Canada. *Water Qual. Res. J. Can.* **34**, 221–247.

Honeyman J. T. and Santschi P. H. (1991) Coupling adsorption and particle aggregation laboratory studies of "colloidal pumping" using "Fe-labeled hematite. *Environ. Sci. Technol.* **25**, 1739–1747.

Hongshao Z. and Stanforth R. (2001) Competitive adsorption of phosphate and arsenate on goethite. *Environ. Sci. Technol.* **35** (24), 4753–4757.

Huerta-Diaz M. A., Tessier A. and Carignan R. (1998) Geochemistry of trace metals associated with reduced sulfur in freshwater sediments. *Appl. Geochem.* **13**(2), 213–233.

Joseph S., Visalakshi G., Venkateswaran G. and Moorthy P. N. (1996) Dissolution of haematite in citric acid-EDTA-ascorbic acid mixtures. *J. Nucl. Sci. Technol.* **33**(6), 479–485.

Kipp G. G., Stone J. J. and Stetler L. D. (2009) Arsenic and uranium transport in sediments near abandoned uranium mines in Harding County, South Dakota. *Appl. Geochem.* **24**(12), 2246–2255.

Laird K. R., Das B. and Cumming B. F. (2014) Enrichment of uranium, arsenic, molybdenum, and selenium in sediment cores from boreal lakes adjacent to northern Saskatchewan uranium mines. *Lake Reserv. Manag.* **30** (4), 344–357.

Langmuir D. (1978) Uranium solution-mineral equilibria at low temperatures with applications to sedimentary ore deposits. *Geochim. Cosmochim. Acta* **42**(6), 547–569.

Larios R., Fernández-Martínez R. and Rucandio I. (2013) Assessment of a sequential extraction procedure for arsenic partitioning and application to samples from different pollution sources. *Anal. Methods* **5**(16), 4096–4104.

Larsen F. and Postma D. (1997) Nickel mobilization in a groundwater well field: release by pyrite oxidation and desorption from manganese oxides. *Environ. Sci. Technol.* **31**(9), 2589–2595.

Li X., Coles B. J., Ramsey M. H. and Thornton I. (1995) Sequential extraction of soils for multielement analysis by ICP-AES. *Chem. Geol.* **124**(1), 109–123.

Liger E., Charlet L. and Van Cappellen P. (1999) Surface catalysis of uranium (VI) reduction by iron (II). *Geochim. Cosmochim. Acta* **63**(19), 2939–2955.

Meyers P. A. and Ishiwatari R. (1993) The early diagenesis of organic matter in lacustrine sediments. In *Organic Geochemistry, Topics in Geobiology* (eds. M. H. Engel and S. A. Macko). Springer, Boston, MA, USA, pp. 185–209.

Minnow Environmental (2019) Mary River project 2017-2018. Lake sedimentation monitoring report. Minnow Environmental Inc., Georgetown, ON, Canada.

Morrison S. J. and Spangler R. R. (1992) Extraction of uranium and molybdenum from aqueous solutions: A survey of industrial materials for use in chemical barriers for uranium mill tailings remediation. *Environ. Sci. Technol.; (United States)* **26** (10), 1922–1931.

Nelson D. M., Penrose W. R., Karttunen J. O. and Mehlhaff P. (1985) Effects of dissolved organic carbon on the adsorption properties of plutonium in natural waters. *Environ. Sci. Technol.* **19**(2), 127–131.

Neves O. and Matias M. J. (2008) Assessment of groundwater quality and contamination problems ascribed to an abandoned uranium mine (Cunha Baixa region, Central Portugal). *Environ. Geol.* **53**(8), 1799–1810.

Olds T. A., Plášil J., Kampf A. R., Škoda R., Burns P. C., Čejka J., Bourgoin V. and Boulliard J. C. (2017) Gauthierite, KPb [(UO2) 7O5 (OH) 7]· 8H2O, a new uranyl-oxide hydroxy-hydrate mineral from Shinkolobwe with a novel uranyl-anion sheet-topology. *Eur. J. Mineral.* **29**(1), 129–141.

Ondrus P., Veselovsky F., Hlousek J., Skala R., Vavrin I., Fryda J., Cejka J. and Gabasova A. (1997) Secondary minerals of the Jáchymov (Joachimsthal) ore district. *J. Geosci.* **42**(4), 3–76.

Pelletier C. A., Wen M. E. and Poling G. W. (2009) Flooding pit lakes with surface water. In *Mine Pit Lakes – Characteristics, Predictive Modeling and Sustainability* (eds. D. N. Castendyk and L. E. Eary). Society for Mining, Metallurgy and Exploration, Littleton, Colorado, USA, pp. 239–248.

Perry D. L., Klainer S. M., Bowman H. R., Milanovich F. P., Hirschfeld T. and Miller S. (1981) Detection of ultratrace levels of uranium in aqueous samples by laser-induced fluorescence spectrometry. *Anal. Chem.* **53**(7), 1048–1050.

Pichler T., Hendry M. J. and Hall G. E. M. (2001) The mineralogy of arsenic in uranium mine tailings at the Rabbit Lake In-pit Facility, northern Saskatchewan, Canada. *Environ. Geol.* **40**(4–5), 495–506.

Pieters R. and Lawrence G. A. (2014) Physical processes and meromixis in pit lakes subject to ice cover. *Can. J. Civ. Eng.* **41**(6), 569–578.

Plášil J. (2014) Oxidation-hydration weathering of uraninite: the current state-of-knowledge. *J. Geosci.* **59**(2), 99.

Pokrovsky O. S., Dupré B. and Schott J. (2005) Fe–Al–organic colloids control of trace elements in peat soil solutions: results of ultrafiltration and dialysis. *Aquat. Geochem.* **11**(3), 241–278.

Poulton S. W. and Canfield D. E. (2005) Development of a sequential extraction procedure for iron: implications for iron partitioning in continentally derived particulates. *Chem. Geol.* **214**(3–4), 209–221.

Ramos O. E. R., Cáceres L. F., Munoz M. R. O., Bhattacharya P., Quino I., Quintanilla J., Sracek O., Thunvik R., Bundschuh J. and García M. E. (2012) Sources and behavior of arsenic and trace elements in groundwater and surface water in the Poopó Lake Basin, Bolivian Altiplano. *Environ. Earth Sci.* **66**(3), 793–807.

Ravel B. and Newville M. (2005) ATHENA, ARTEMIS, HEPHAESTUS: data analysis for X-ray absorption spectroscopy using IFEFFIT. *J. Synchrotron. Radiat.* **12**(4), 537–541.

Rogozin D., Zadereev E., Prokopkin I., Tolomeev A., Barkhatov Y., Khromechek E., Degermendzhi N., Drobotov A. and Degermendzhi A. (2017) Comparative study of the stability of stratification and the food web structure in the meromictic lakes Shira and Shunet (South Siberia, Russia). In *Ecology of Meromictic Lakes* (eds. R. D. Gulati, E. S. Zadereev and A. G. Dgermendzhi). Springer, Cham, Switzerland, pp. 89–124.

Ross J. M. and Sherrell R. M. (1999) The role of colloids in tracemetal transport and adsorption behavior in New Jersey Pinelands streams. *Limnol. Oceanogr.* **44**(4), 1019–1034.

Ryan J. N. and Elimelech M. (1996) Colloid mobilization and transport in groundwater. *Colloids Surf.: Physicochem. Eng. Aspects* **107**, 1–56.

Saunders J. A., Lee M. K., Dhakal P., Ghandehari S. S., Wilson T., Billor M. Z. and Uddin A. (2018) Bioremediation of arsenic-contaminated groundwater by sequestration of arsenic in biogenic pyrite. *Appl. Geochem.* **96**, 233–243.

Sheppard M. I. and Thibault D. H. (1992) Desorption and extraction of selected heavy metals from soils. *Soil Sci. Soc. Am. J.* **56**(2), 415–423.

Slowey A. J., Johnson S. B., Newville M. and Brown G. E. (2007) Speciation and colloid transport of arsenic from mine tailings. *Appl. Geochem.* **22**(9), 1884–1898.

Soni A., Mishra B. and Singh S. (2014) Pit lakes as an end use of mining: A review. *Int. J. Min. Reclam. Environ.* **5**(2), 99–111.

Tamura N. (2014) XMAS: A versatile tool for analyzing synchrotron X-ray microdiffraction data. In *Strain and Dislocation Gradients from Diffraction – Spatially-Resolved Local Structure and Defects* (eds. R. Barabash and G. Ice). World Scientific Publishing Co Pte Ltd., pp. 125–155.

Tang Y. and Reeder R. J. (2009) Enhanced uranium sorption on aluminum oxide pretreated with arsenate. Part I: Batch uptake behavior. *Environ. Sci. Technol.* **43**(12), 4446–4451.

Tessier A., Campbell P. G. and Bisson M. (1979) Sequential extraction procedure for the speciation of particulate trace metals. *Anal. Chem.* **51**(7), 844–851.

Tranvik L. (1994) Effects of colloidal organic matter on the growth of bacteria and protists in lake water. *Limnol. Oceanogr.* **39**(6), 1276–1285.

Troyer L. D., Stone J. J. and Borch T. (2014) Effect of biogeochemical redox processes on the fate and transport of As and U at an abandoned uranium mine site: an X-ray absorption spectroscopy study. *Environ. Chem.* **11**(1), 18–27.

Vail J. (2013) Groundwater sampling. Operating procedure. U.S. Environmental Protection Agency Science and Ecosystem Support Division. Athens, Georgia. URL www.epa.gov/sites/production/files/2015-06/documents/Groundwater-Sampling.pdf.

van Emden B., Thornber M. R., Graham J. and Lincoln F. J. (1997) The incorporation of actinides in monazite and xenotime from placer deposits in Western Australia. *Can Mineral* **35**(1), 95–104.

Vandenhove H., Vanhoudt N., Duquène L., Antunes K. and Wannijn J. (2014) Comparison of two sequential extraction procedures for uranium fractionation in contaminated soils. *J. Environ. Radioact.* **137**, 1–9.

von Gunten H. R., Sturm M. and Moser R. N. (1997) 200-year record of metals in lake sediments and natural background concentrations. *Environ. Sci. Technol.* **31**(8), 2193–2197.

von Gunten K., Alam M. S., Hubmann M., Ok Y. S., Konhauser K. O. and Alessi D. S. (2017) Modified sequential extraction for biochar and petroleum coke: Metal release potential and its environmental implications. *Bioresour. Technol.* **236**, 106–110.

von Gunten K., Warchola T., Donner M., Cossio M., Hao W., Boothman C., Lloyd J., Siddique T., Partin C. A., Flynn S., Rosaasen A., Konhauser K. O. and Alessi D. S. (2018) Biogeochemistry of U, Ni, and As in two meromictic pit lakes at the Cluff Lake uranium mine, northern Saskatchewan. *Can. J. Earth Sci.* **55**(5), 463–474.

von Gunten U. and Schneider W. (1991) Primary products of the oxygenation of iron (II) at an oxic—anoxic boundary: Nucleation, aggregation, and aging. *J. Colloid Interface Sci.* **145**(1), 127–139.

Wang C. F., Jeng S. L. and Shieh F. J. (1997) Determination of arsenic in airborne particulate matter by inductively coupled plasma mass spectrometry. *J. Anal. At. Spectrom.* **12**(1), 61–67.

Wang Y., Frutschi M., Suvorova E., Phrommavanh V., Descostes M., Osman A. A., Geipel G. and Bernier-Latmani R. (2013) Mobile uranium (IV)-bearing colloids in a mining-impacted wetland. *Nat. Commun.* **4**, 2942.

Warner J. and Rowson J. (2007) Technical report: in-situ monitoring and validation of a uranium mill tailings management facility design using X-ray absorption near edge structure (XANES) spectroscopy. *Synchrotron Radiat. News* **20**(3), 14–17.

Wielinga B., Bostick B., Hansel C. M., Rosenzweig R. F. and Fendorf S. (2000) Inhibition of bacterially promoted uranium reduction: Ferric (hydr)oxides as competitive electron acceptors. *Environ. Sci. Technol.* **34**(11), 2190–2195.

Wilmarth W. R., Mills J. T., Dukes V. H. and Sullivan R. C. (2006) Effects of in-tank precipitation of sodium aluminosilicate on uranium chemistry. *Sep. Sci. Technol.* **41**(11), 2325–2340.

Yang B., Tong X., Deng Z. and Lv X. (2016) The adsorption of Cu species onto pyrite surface and its effect on pyrite flotation. *J. Chem. (Hindawi. Online)*, id4627929.

Associate editor: Karen Johannesson